



**BE CIVIL ENGINEERING
PROJECT REPORT**

**Modified Design of Monopiles for the offshore wind turbines (OWT) in the
coastal areas of Pakistan**

**Project submitted in partial fulfilment of the requirements for the degree
of
BE Civil Engineering**

PROJECT ADVISOR

Lt. Col. Dr. Naveed Metla

PROJECT CO-ADVISOR

AP Dr. Muhammad Bilal Adeel

SYNDICATE MEMBERS

Muhammad Usama khan (Syndicate Leader)	293927
Muhammad Sayyam Asif	290289
Muhammad Abdullah	298126
Abdul Muhaimin Jamil	287028
Zia Ur Rehman	297400
Ali Hassan	309533

MILITARY COLLEGE OF ENGINEERING
NATIONAL UNIVERSITY OF SCIENCES & TECHNOLOGY
RISALPUR CAMPUS, PAKISTAN

(2023)

**This is to certify that the
BE Civil Engineering Project entitled**

**Modified Design of Monopiles for the offshore wind turbines (OWT) in the
coastal areas of Pakistan**

SUBMITTED BY

CMS-293927 Muhamad Usama Khan (Syndicate leader)

CMS-290289 Muhammad Sayyam Asif

CMS-298126 Muhammad Abdullah

CMS-287028 Abdul Muhaimin Jamil

CMS-297400 Zia Ur Rehman

CMS-309533 Ali Hassan

Has been accepted towards the partial fulfilment of the
requirement for BE Civil Engineering Degree

Lt. Col. Dr. Naveed Metla

(Syndicate Advisor) Associate Professor

Military College of Engineering (MCE),

National University of Sciences and Technology (NUST),

Dedication

We dedicate this research to our beloved PARENTS and respected INSTRUCTORS, who prayed for us, and gave us encouragement and moral support throughout our endeavor.



Abstract:

The famous American Petroleum Institute (API) method is used commonly for the design of small diameter piles. This method does not incorporate the effect of large diameter and overturning moments of monopiles. The present study deals with design of the Monopile foundation for offshore wind turbine farms in the coastal areas of Pakistan. ABAQUS FEA software is used to simulate specimens that are subjected to surface lateral loads. While taking into account different structural and environmental factors, including aerodynamic and hydrodynamic forces, a nonlinear static analysis of the substructure is performed. Various configurations of hollow monopile are studied through parametric analysis, by changing water depths and soil properties. Design involves a 3D model of monopile of diameter 3m ,5m ,7m, while treating the soil of the seabed as a non-linear three-dimensional material. Soil is modeled by Mohr Coulomb criteria. As a result, p - y curves are generated. This study particularly recommends a specific diameter for the monopiles for the installation of OWTs in the coastal areas of Karachi and Gwadar based on its impact on lateral response and structural stability. The proposed model was also validated with an experimental and numerical result of China based Offshore wind turbines that confirmed the accuracy of the numerical model's predictions.

Contents

ACKNOWLEDGEMENTS	13
COPYRIGHT NOTICE	14
Chapter 1	15
1.1 Introduction:	15
1.2 Problem Statement:	16
1.3 Research Gaps:	17
1.4 Available Methods for design:.....	18
1.5 Research Objective:	18
1.6 The thesis format:	18
Chapter 2 Literature Review	20
2.1 General	20
2.2 Beam on Winkler Foundation (BNWF) Approach	22
2.2.1 Numerical stimulation of p-y model under monotonic loading	22
2.2.2 Generalized analysis of the nonlinear soil structure interaction using the Winkler model.	22
2.2.3 Analysis of nonlinear seismic response of a single sand pile	23
2.3 Numerical Study	26
2.3.1 Numerical analysis of long-term performance of monopile-supported offshore wind turbines:	26
2.3.2 Numerical simulation of Monopiles in Dense Sand:.....	27
2.3.3 FEM of lateral loaded monopile in non-homogenous clay:.....	28
2.4 Experimental Study	30
2.4.1 Experimental generation of p-y curves for Large-Diameter Monopiles in Sands: Centrifuge Tests	30
2.5 Properties of Sand at seabed of Pakistan	34
Chapter 3 Methodology	36
3.1 General	36
3.2 Finite Element Model Parts:	36
3.2.1 Pile Modelling:.....	36
3.2.2 Soil Modelling:	37
3.2.3 FE-Mesh:	39
3.2.4 Pile-soil interaction:	40
3.2.5 Boundary Conditions:.....	40
3.2.6 Loading:.....	41
3.2.7 Steps:	41

3.3 Statistical Analysis:.....	42
Chapter 4 Results	44
4.1 FEM Analysis of 3m diameter:.....	44
4.1.1 General Properties	44
4.1.2 Relationship between Depth and Bending Moment	46
4.1.3 Relationship between depth and displacement.....	49
4.1.4 <i>P-Y</i> Curves	51
4.2 FEM Analysis of 5m diameter:.....	53
4.2.1 General Properties	53
4.2.2 Relationship between Depth and Bending Moment	56
4.2.3 Relationship between depth and displacement.....	57
4.2.4 <i>P-Y</i> Curves	59
4.3 FEM Analysis of 7m diameter:.....	61
4.3.1 General Properties	61
4.3.2 Relationship between depth and bending moment	64
4.3.3 Relationship between depth and displacement.....	66
4.1.4 <i>P-Y</i> Curves	69
Chapter 5 Recommended equation	72
5.1 Parameters for 3 m	72
5.2 Parameters for 5m	73
5.3 Parameters for 7m	74
5.4 Equation	75
Chapter 6 Validation	76
6.1 Aims and Objectives of Validation:	76
6.2 Finite Element Analysis:	76
6.3 Soil Modelling	77
6.4 Pile Modelling	77
6.5 FE Mesh	78
6.6 Loading:	79
6.7 Boundary Conditions	79
6.8 Comparison of Experimental and FEA results:	80
6.8.1 Relationship between depth and bending moment	80
6.8.2 Relationship between depth and displacement.....	80
6.8.3 <i>P-Y</i> Curves	81

6.9 Results and analysis	82
Chapter 7 Conclusion	84
7.1 Relationship between depth and bending Moment:	84
7.2 Relationship between depth and displacement:	84
7.3 Relationship between soil resistance and displacement:	84
7.4 Potential Contributions:.....	84
7.5 Future Outlook.....	85
Chapter 8 References:	87

List of Figures

Figure 1: Share of renewable energy and non-renewable energy resources in production of electricity in Pakistan	16
Figure 2: Various types of Foundation	16
Figure 3: Offshore Wind Turbine System Sustainability Analyses (US Department of Energy)	17
Figure 4: Computed and measured time-history response of super structure	23
Figure 5: Spectrum response of Northridge earthquake at bedrock	24
Figure 6: Comparisons of peak displacements and bending moments computed and observed	24
Figure 7: A comparison of estimated and measured: a) maximum deformation, and b) Bending moment distribution	25
Figure 8: The pile's lateral strength as determined by pushover and seismic analysis	25
Figure 9: Three types of 3D FEM were built: (a) Entire model; (b) pile-soil interaction with consideration for long-term effects; and (c) pile-soil interaction without such considerations	26
Figure 10: Mesh details (a) test pile 1; (b) test pile 2	27
Figure 11: FEM of Pile	29
Figure 12: Failure Mechanism of Monopile Foundation	30
Figure 13: Schematic diagram of centrifuge test	31
Figure 14: Bending moment distribution	32
Figure 15: Comparison between experimental p-y data points and the Reese and the API p-y curves	33
Figure 16: Monopile schematic and parametrized diagram for dimensions	38
Figure 17: Boundary Conditions	40
Figure 18: Abaqus Modelling steps	42
Figure 19: The 40 layers of the soil from top to bottom with increasing elastic modulus	44
Figure 20: FEM Mesh	45
Figure 21: Relationship between Depth and Bending Moment for angle of internal friction 30°	46
Figure 22: Relationship between Depth and Bending Moment for angle of internal friction 35°	47
Figure 23: Relationship between depth and bending Moment for angle of internal friction 40°	48
Figure 24: Relationship between depth and displacement for angle of internal friction 30°	49
Figure 25: Relationship between depth and displacement for angle of internal friction 35°	50
Figure 26: Relationship between depth and displacement for angle of internal friction 40°	51
Figure 27: P-Y Curves for the angle of internal friction of 30°	52
Figure 28: P-Y Curves for the angle of internal friction of 30°	52
Figure 29: P-Y Curves for the angle of internal friction of 40°	53
Figure 30: 40 layers of the soil from top to bottom with increasing elastic modulus	54
Figure 31: FEM Mesh	55
Figure 32: Relationship between depth and bending Moment for angle of internal friction 30°	56
Figure 33: Relationship between depth and bending Moment for angle of internal friction 35°	56
Figure 34: Relationship between depth and bending Moment for angle of internal friction 40°	57
Figure 35: Relationship between depth and displacement at the angle of internal friction 30°	58
Figure 36: Relationship between depth and displacement at the angle of internal friction 35°	58

Figure 37: Relationship between depth and displacement at the angle of internal friction 40°	59
Figure 38: P-Y Curves for the angle of internal friction 30°	60
Figure 39: P-Y Curves for the angle of internal friction 35°	60
Figure 40: P-Y Curves for the angle of internal friction °40°	61
Figure 41: 40 layers of the soil from top to bottom with increasing elastic modulus	62
Figure 42: FEM Mesh	63
Figure 43: Relationship between bending moment and depth for angle of interna Ifriction 30°	64
Figure 44: Relationship between bending moment and depth for angle of interna Ifriction 35°	65
Figure 45: Relationship between bending moment and depth for angle of interna Ifriction 40°	66
Figure 46: Relationship between depth and displacement at for angle of internal friction 30°	67
Figure 47: Relationship between depth and displacement at for angle of internal friction 35°	68
Figure 48: Relationship between depth and displacement at for angle of internal friction 40°	69
Figure 49: P-Y Curves for the angle of internal friction 30°	70
Figure 50: P-Y Curves for the angle of internal friction 35°	70
Figure 51: P-Y Curves for the angle of internal friction 40°	71
Figure 52: Layers of soil	77
Figure 53: Finite element mesh	78
Figure 54: Comparison of bending moment and depth curve between the experimental study results and Finite element analysis results	80
Figure 55: Comparison of depth and displacement curve between the experimental study results and Finite element analysis results	81
Figure 56: Comparison of p-y curves of experimental study and Finite element analysis	82

List of Tables

Table 1: Pile geometries for FEM	37
Table 2: Soil profile and soil parameters used for FE-modelling for $\Phi=30$ degree	39
Table 3: Soil parameters used for FE-modelling	39
Table 4: load applied for FEM	41
Table 5: Properties of pile for 3m diameter	44
Table 6: Detail of Mesh for 3m diameter	45
Table 7: Properties of pile for 5m diameter	54
Table 8: Detail of Mesh for 5m diameter	55
Table 9: Properties of piles for 7m diameter	62
Table 10: Detail of Mesh for 7m diameter	63
Table 11: Permissible values of constants a and b in the general form of equation of best fit	73
Table 12: The values of statistical parameters to justify the correctness of the results	73
Table 13: Permissible values of constants a and b in the general form of equation of best fit	73
Table 14: The values of statistical parameters to justify the correctness of the results	74
Table 15: Permissible values of constants a and b in the general form of equation of best fit	74
Table 16: The values of statistical parameters to justify the correctness of the results	74
Table 17: Properties of sand and clay from experimental study	77
Table 18: Properties of pile from experimental study	78
Table 19: Mesh Details from experimental study	79
Table 20: Loadings from experimental study	79

ACKNOWLEDGEMENTS

We completed this research endeavor by the mercy of Almighty Allah, and we cannot thank Him enough for bestowing upon us the power and intelligence to do so. Since the inception of the universe, the Holy Prophet (P.B.U.H) has been a source of inspiration for all humanity. We extend our sincere admiration and gratitude to him. We are extremely grateful to our parents, whose steadfast support and encouragement have formed the firm foundation of our personal, professional, and educational life. We would also like to thank our respected instructors, especially our Project supervisor Dr Naveed Metla and Co-advisor Assistant Professor Dr. Bilal Adeel, for their unwavering support and encouragement throughout the research. Their continuous support and guidance have served as a continual source of inspiration for us. We would like to use this opportunity to extend our sincere gratitude once again to everyone who has helped us to make this endeavor a success

COPYRIGHT NOTICE

This thesis and all of its components are written under a copyright licence. Without the author's clear written consent, it is completely forbidden to use this thesis, in whole or in part, to create a derivative work. This thesis may be used for non-commercial purposes in whole or in part, as long as the author is fully credited.

@ 2023 ALL RIGHTS RESERVED

Chapter 1

1.1 Introduction:

One of Pakistan's biggest problems is the energy crisis. Pakistan faces an electricity shortfall of approximately 6500 MW. Nowadays, Pakistan relies on non-renewable resources mainly, imported fuel and coal which are very costly, figure 1 shows the share of different resources that are being used to produce electricity. The world is now moving towards the use of renewable sources like solar and wind energy to produce electricity and meet their energy needs. Wind energy is a significant source of production of electricity. The coastline of Pakistan is 1001 km long, and include two major cities, Karachi and Gwadar. Our coastline is virgin and undeveloped. Offshore wind turbine farms along the coastline can help Pakistan to minimize the energy crisis. There are numbers of foundation concepts available for OWTs, such as tripod, bucket, gravity and monopiles shown in figure 2. A steel pile with an open end that resembles a pipe and has a larger diameter ranging from 3 to 7 meters is referred to as monopile foundation. Foundations are considered the base of a structure, monopile can be an excellent choice. The loads being applied on the turbine are transmitted to the soil strata of sea. therefore the monopile foundation will play a significant role in that load transmission. The average design life of turbine is 20 to 25 years, and these complex systems are put through significant high cyclic lateral loadings and overturning moments due to waves, wind blade rotation or even seismic origin which are varying in amplitude, direction, and frequency. According to the reports from Pakistan Meteorological Department (PMD) and National renewable Energy laboratory reports, Pakistan has a huge wind potential and could produce 132 GW of electricity from wind and solar resources. Reducing the effect of global warming is one of the major issues for which numerous steps are being taken. In order to add our efforts to this cause we have planned to design a monopile foundation for Offshore wind turbines farms for Pakistan. United Nations Sustainable Development Goals that are linked to the proposed project include the; Affordable and clean energy (Goal number 7), Industry, innovation and infrastructure (Goal number 9), sustainable cities and communities (Goal number 11) and, Climate action (Goal number 13)

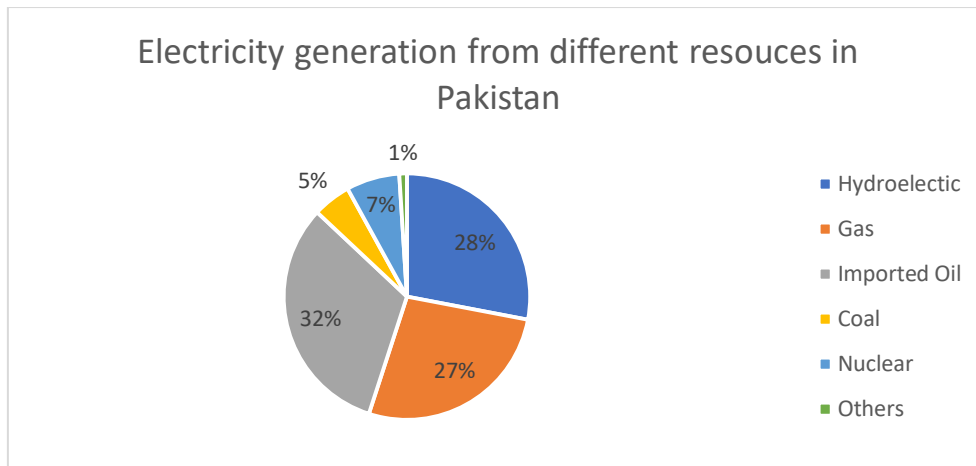


Figure 1: Share of renewable energy and non-renewable energy resources in production of electricity in Pakistan

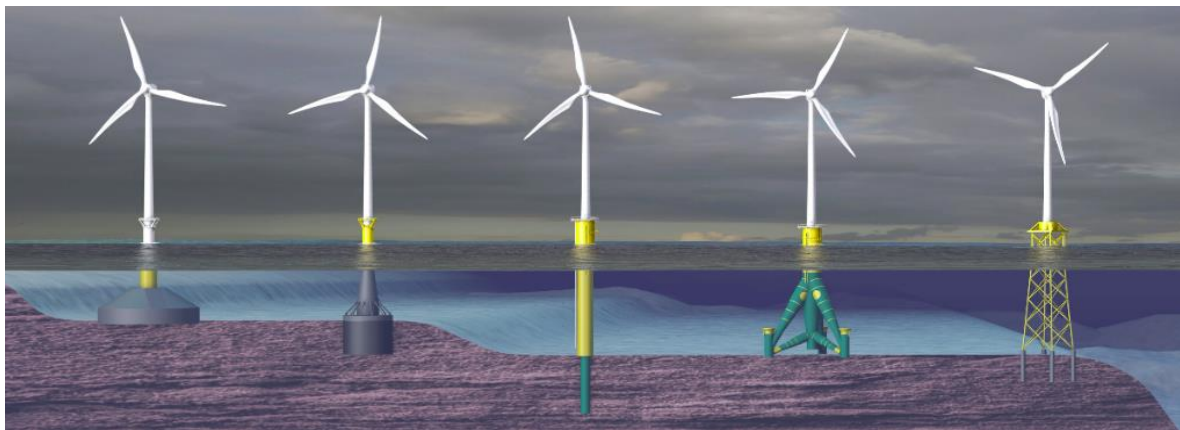


Figure 2: Various types of offshore wind turbine foundations

1.2 Problem Statement:

Monopile foundation is in limelight in developed and developing countries since long, for wind turbine farms and other offshore structures. Monopiles are currently designed using a semi-empirical method called *the p-y* method. Various codes like American Petroleum Institute (API) and Det Norske Veritas (DNV) codes have adopted this method. The *p-y* method is extracted from field tests conducted on small diameter monopiles. These methods have some shortcomings; Firstly they focus on the design of piles of smaller diameter. Secondly, these methods overestimate the bending moments and lastly, pile rotation (rather than deflection) is neglected which is more prominent for foundations of offshore structures. These methods do not incorporate the distribution of moments at soil-pile interface and the Base shear and Base moment reactions of the soil. These shortcomings make the structures uneconomical. The lateral loads applied to a monopile create a lateral monopile deflection and lateral soil resistance in the surrounding soil. It is a necessity to precisely compute the lateral monopile deflection and soil resistance in order to perform an accurate monopile design. Thus, for large diameter

monopiles, the p - y method cannot be used with confidence and needs to be validated. To overcome this problem, three dimensional (3D) numerical modelling based on finite element method are considered significant in regard to large diameter monopiles.

Recently, US department of Energy has given a report about the use of Wind energy to produce electricity in the world, figure 3 shows the already announced offshore wind projects around the world mounting up to 29GW of new capacity in 2026. Being the 3rd largest country in Asia, it is our prime responsibility to look forward to this dimension of production of electricity using wind energy. Other Asian countries has already taken steps to use wind energy to meet their energy needs, Pakistan has high potential of production of energy using Wind, so this issue is to be addressed at a foremost priority.

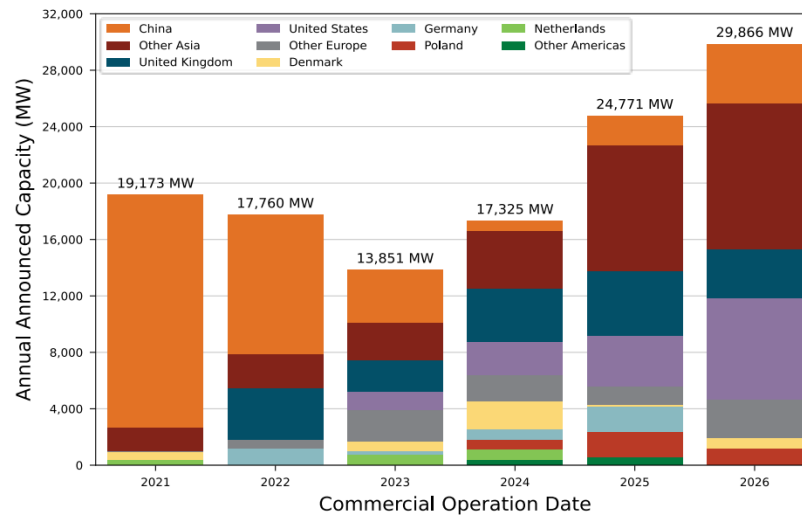


Figure 3: Offshore Wind Turbine System Sustainability Analyses (US Department of Energy)

1.3 Research Gaps:

The potential research gaps in regard to monopile foundation design for OWTs in Pakistan include need for:

- a) Development of *soil reaction and displacement (p-y)* curves for larger monopile using numerical methods that consider the various constitutive models of soil.
- b) Considering the site-specific wind and wave speed to consider the exact loading conditions.
- c) Soil-pile interface interaction is especially important parameter to study soil reaction this should be considered for further researches
- d) Scouring and corrosion properties of the pile.
- e) Limited research on the structural and physical parameters
- f) Experimental testing and studies for the scaled-down models and prototypes of the monopile.

1.4 Available Methods for design:

There are number of methods used to design monopiles for OWTs, including:

- a) Beam on Winkler foundation (BNWF) model: This method focuses on pile being used in the form of simple beam and seabed soil is modelled with springs with various spring like properties to judge the structural integrity of piles
- b) American Petroleum Institute (API) method: This method is adopted particularly for the oil and gas offshore structures. The method is more like a set of rules and guidelines for the design procedure. The method describes the limit states of piles and pile groups
- c) Eurocode 7: This is a code stating the limit states for monopile design in the European states, the code considers the soil of all the coastlines of Europe.
- d) *P-Y* Curves method: This is a semi-empirical method in which soil resistance and displacement graphs are plotted to observe the response of soil and pile. The method is used with greater agreement for smaller diameter piles.
- e) Finite Element Analysis: This is a numerical method which uses various software like ABAQUS, LPILE and many others to perform the analysis and generate the results

The application of each of the methods has its merits and demerits. The use of a particular method depends on the site-specific data, soil parameters and also the application for various data analytic tools and empirical relationships.

1.5 Research Objective:

The aim of our study is to design the Monopile foundation. For this following objective are identified:

- a) To evaluate the performance of 3D model of monopile using Finite element analysis (FEA) with ABAQUS.
- b) To generate *soil-reaction and lateral displacement* $-(p-y)$ curves at various depths.
- c) To validate the result of experimental study by FEA.
- d) To recommend numerically modelled parametric equations for large diameter monopiles.

1.6 The thesis format:

The thesis has been arranged in eight chapters: -

- **Chapter 1: Introduction**, this chapter gives a general introduction to the offshore wind energy, objectives, and problem statement, research objectives and available approaches to design monopiles

- **Chapter 2: Literature Review**, this chapter gives a brief discussion of offshore wind turbines problems and reviews the researches which has been conducted during the last decade on experiment and numerical investigation. It gives detailed explanation of numerical simulation which this research is based on.
- **Chapter 3: Methodology 3D Finite Element monopiles modelling using Abaqus 6.14**, this chapter deals with numerical modelling Particularly, it describes the way how data is collected, and the equations used to extract empirical and parametric results Finite element analysis (FEA) large diameter monopiles is presented, and its implementation in this study is elaborated. It also shows the use of origin pro to build the final parametric equations using statistical analysis.
- **Chapter 4: Result of the analysis**, the chapter focuses on the result and graphs obtained and analysis the results. The suitable reason for a particular domain is discussed briefly in the chapter. A wide parametric study, for the impact of loads on the monopile behavior, is presented in this chapter.
- **Chapter 5: Recommended Equations**, based on the sensitivity analysis done in previous chapters, this chapter presents the details of the followed technique of adapting and developing the equation, which is applicable until diameter 7m that will be required to support greater offshore structure, which is need of the time to enhance the use of clean energy sources.
- **Chapter 7: Conclusions**, A summary of the work done in numerical modeling, conclusions and the recommendations of this study are drawn in this chapter. Publications and a scope for future work are also included.
- **Chapter 8: References**, Some notable researchers and researches are mentioned in this chapter sued so far to perform our study

Literature Review

Several researches have been done to analyze the performance of monopile foundations under various states and using different approaches. Some of them are discussed in detail in the subsequent sections.

2.1 General

Use of monopile foundations for OWTs has increased manifolds throughout the world due to their efficiency and affordability. According to Goupee et al. (2016), monopiles are usually made of steel and have a large diameter to provide sufficient support for the turbine structure.

Consequently, due to the boom in oil gas sector in the offshore platforms in 1950, Number of studied has been performed to analyze the performance of laterally loaded piles. Various empirical studies proposed the equation to accurately determine the ultimate soil resistance to design the monopile. *Broms et al. (1964)* ignored rotation of pile and assumed that the soil resistance was distributed in one direction only. *Hanson et al. (1961)* and *Meyerhof et al (1981)*, they studied the response and distribution of the soil resistance and showed it has various prospects which need to be perceived while designing. *Prasad and Chari et al. (1999)*, their numerical stimulation has shown that the results of soil resistance can be used in greater agreement with the testing results. Various codes like API and DNV consider the effect of normal and shear stresses around laterally loaded monopiles.

One major concern is that the stiffness parameter of soil and pile can be found by investigation, and they are known but the stiffness parameters of soil-pile interface are unknown. To solve this problem, several experimental studies have been conducted and different equations have been derived to find the soil pressure on monopile.

The evolution in the p - y curve method in regard to monopiles is described below:

- a) *Winkler et al* introduced the basic BNWF method in which soil is modelled with uncoupled springs and the pile is modelled as flexible beam.
- b) *Hetenyi et al. (1946)* introduced the concept of beam on an elastic foundation, a modification to BNWF approach.
- c) *McClelland et al. (1958)* and *Reese and Matlock (1956)* proposed the basic equations of p - y curve method which are still in use and many researchers suggest changes to these basic equations.

- d) *Matlock et al. (1970)* studied the dependence of soil resistance at depth and showed after a particular point of depth the behavior of soil resistance changes.
- e) *Cox et al. (1966)* used fully instrumented monopiles at Mustang Island and tests were conducted on site
- f) *Reese et al. (1974)* Based on the Mustang Island test, a semi-empirical p-y curve equation is derived
- g) *O'Neill and Murchison (1983)* derived the modified tangent hyperbolic function of p-y curve method
- h) *O'Neill and Murchison (1984)* compared the p-y curve formulation suggested by *Reese et al. (1974)*, with the equation by *O'Neill and Murchison (1983)* and two optimized expressions by comparing the formulations to a database of lateral monopile load experiments that are generally well-documented. The formulation of *O'Neill and Murchison (1983)* was found to provide better results compared to the original equations formulated by *Reese et al. (1974)*. The equation of *O'Neill and Murchison (1983)* was later adopted by American Petroleum Institute (API) and Det Norske Veritas (DNV).

Monopiles are currently designed using a semi-empirical method (called p-y method). In the present, *Matlock (1970)* research on p-y curves is used for the offshore oil & gas industry to better understand the behavior of long slender laterally loaded monopiles. It is based on field research conducted on small diameter monopiles that ranged between 0.254 and 0.610 m in diameter.

Bukhari et al. (2019) conducted a study to investigate the bearing capacity and settlement of monopiles in sandy soils. The study involved conducting laboratory tests on sandy soil samples and analyzing the results using empirical and analytical methods. According to the findings, bearing capacity and settlement of monopile foundations in sandy soils depends on soil properties and loadings applied. The study concluded that more research is needed to optimize the monopile design and improve its performance in sandy soils.

Khan and Akram (2019) used FEA to examine monopiles in coastal areas of Pakistan. The study involved modeling the monopile foundation using ABAQUS software and analyzing its response to various loading conditions. The outcome was, the monopile foundation is suitable to provide adequate support for the wind turbine structure under the given soil conditions. However, the study highlighted the need for further research to optimize monopile design and improve its performance in the coastal areas of Pakistan.

Rehman et al. (2021) proposed a modified design . The study involved conducting laboratory tests on sandy soil samples and analyzing the results using FEA software. The results showed that the proposed modified design, which involved using a tapered pile section, improved the pile-soil interaction and reduced the stresses on the pile. The study concluded that the modified design could improve the performance of monopiles in sandy soils in the coastal areas of Pakistan.

These findings indicate the necessity for more study to improve the foundation and the difficulties in developing monopile foundations for offshore wind turbines in Pakistani coastal locations.

2.2 Beam on Winkler Foundation (BNWF) Approach

2.2.1 Numerical stimulation of p-y model under monotonic loading

Gil Rueda et al. (2021) proposed a numerical method that combines one-dimensional finite difference modeling and 3D-finite element modeling to examine the behavior of laterally loaded monopiles in sand. The study focused on monopiles embedded in non-cohesive soils on which monotonic horizontal loading was applied. Hyperplastic criteria were used to model the soil behavior, and MATLAB was used to model the monopile using the Beam on Winkler Foundation (BNWF) Approach. Results showed that simplifying pile response as pure rigid or pure flexible is not good for monopiles of large diameter and small values of displacements were obtained at the base of pile even for smaller loads.

2.2.2 Generalized analysis of the nonlinear soil structure interaction using the Winkler model.

The adaptable BNWF stimulation for the investigation of deep and shallow foundations was proposed by Hesham et al. (2008). The model was created as a separate module that may be used with commercial tools for nonlinear structural analysis. The cyclic loading principles, slack section growth, the modelling of cyclic debasement, and radiation sparge are some of characteristics that are described. It was demonstrated that the model is capable of capturing different response aspects seen in SSI tests. Additionally, The model's predictions for centrifuge testing of piles in weakening and partially weakening soil were proven to be in excellent accord with the study outcomes. The results of the two cases' time histories are shown figure 4. For both examples' the acceleration and displacement records' overall trend could be properly predicted. The maximal superstructure accelerations for Csp2_E were 0.21g and 0.18g, respectively, whereas the peak displacement was significantly overestimated. Observed and assumed peak displacements for Csp4_E were 587mm and 593 mm, respectively, while the assumed and measured accelerations were 0.73g and 0.7g, respectively. Near end of the time history (16s), there is a discrepancy in the response that might be caused by resonance impacts.

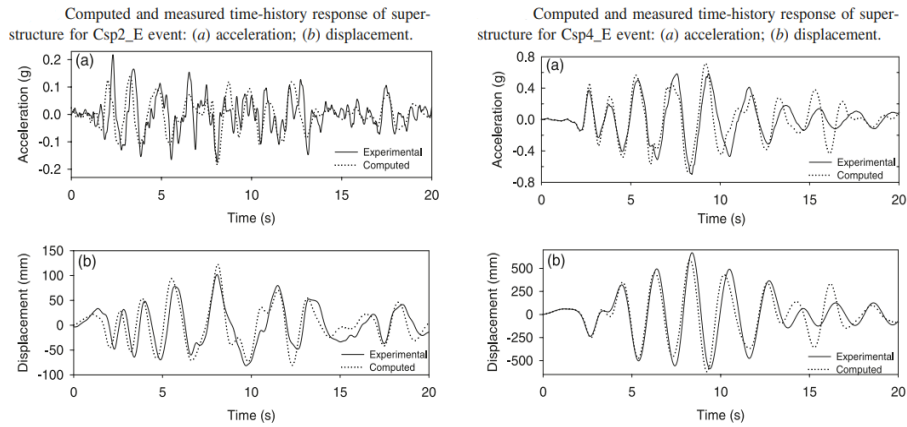
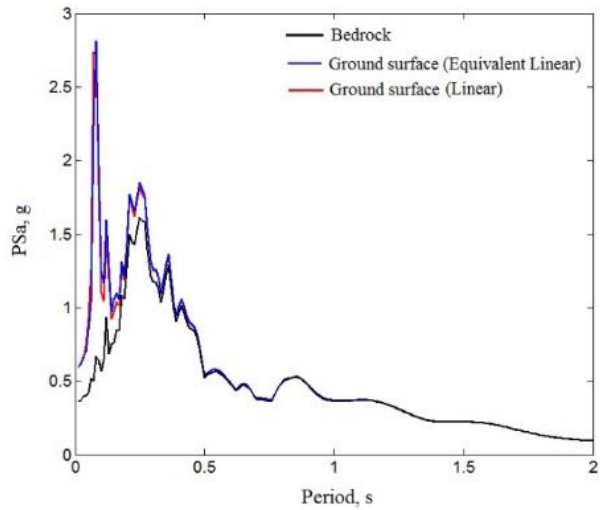


Figure 4: Computed and measured time-history response of super structure

2.2.3 Analysis of nonlinear seismic response of a single sand pile

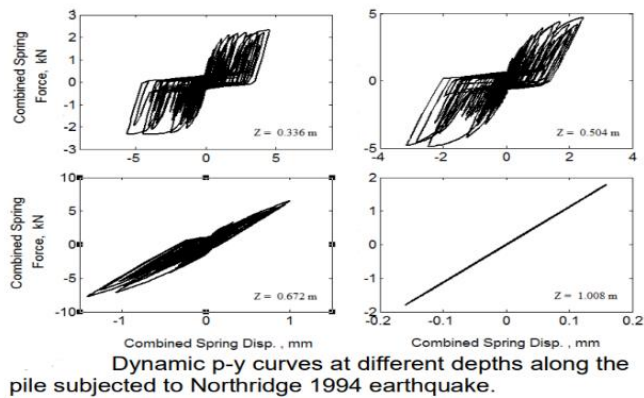
Mehdi et al. (2017) adopted a nonlinear stimulation to perform the seismic analysis of piles under seismic loading. It has the ability to take into consideration key SSI characteristics such like cyclical soil hardening, formation of gaps, and soil cave-in. The analysis is based on a generalized BNWF approach. By contrasting the numerical findings with full-scale test data, the model's predictions' correctness is confirmed. In order to analyse the seismic data from the full-scale test, a dynamic BNWF model was employed. One of the nonlinear BNWF components is linked to each of the pile nodes below the surface of the earth. Free-field ground response studies were conducted using 1D linear (L) and equivalent linear (EL) site response analyses in the frequency domain.

Figure 5 displays that, in the experimental testing, the acceleration response spectrum of the Northridge earthquake from 1994 was applied to base of the shear box. The natural frequency of the soil layer is shown in figure 6 of response spectrum of the acceleration-time history of the ground at surface. The ground responses derived from linear and comparable linear analyses are identical. It has been demonstrated that the BNWF model can reproduce a number of soil-pile interaction characteristics, including the p-y curves at 0.336, 0504, 1.008, 2.672m depths . A static pushover analysis, a typical alternative technique for nonlinear analysis of structures, was also carried out. The pile reaction identified by the pushover investigation matches the lateral displacement of 27.74 mm used at the pile-head .As pile approaches the surface, it deflects significantly



Response Spectrum of Northridge earthquake at bedrock and ground surface for 4.57 m of sand soil.

Figure 5: Spectrum response of Northridge earthquake at bedrock



Dynamic p-y curves at different depths along the pile subjected to Northridge 1994 earthquake.

Figure 6: Comparisons of peak displacements and bending moments computed and observed

The assumed maximum bending moment is nearly 20% lower than the measured value as shown in Figure 7 but the calculated structural reaction of the pile due to vibration are similar.

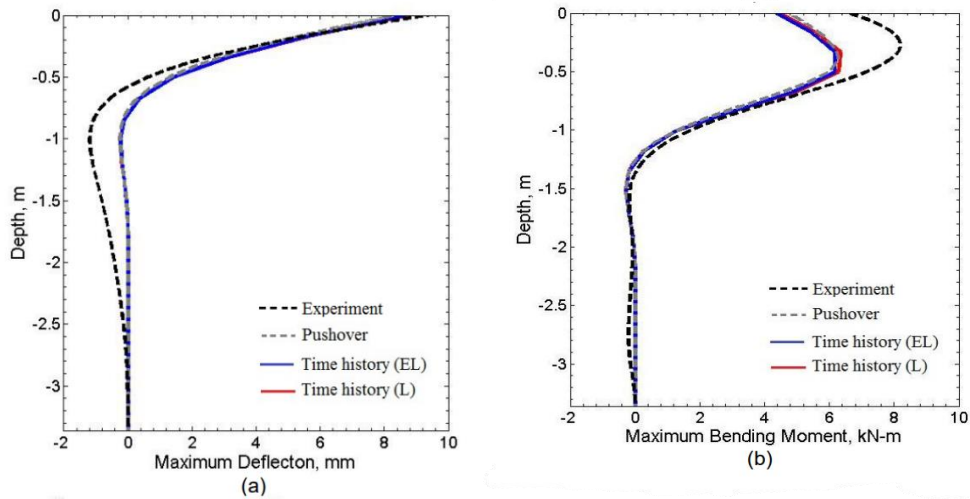


Figure 7: A comparison of estimated and measured: a) maximum deformation, and b) Bending moment distribution

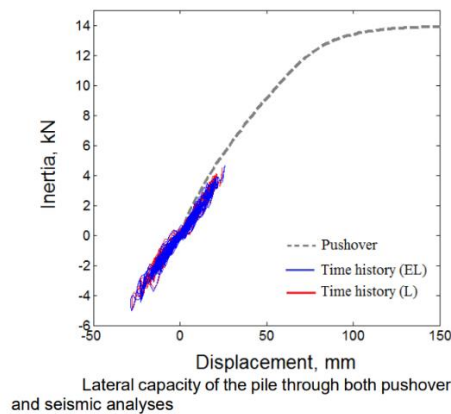


Figure 8: The pile's lateral strength as determined by pushover and seismic analysis

Figure 8 shows the inertia forces for pushover and dynamic analyses displayed against pilehead displacements. This demonstrates that the applied earthquake caused induced shear stresses inside the 4.7 m depth soil layers within the specified range, producing identical side-to-side ground excitations. With fair accuracy, In the same soil conditions, the nonlinear response of a pile might be predicted using the pushover analysis.

2.3 Numerical Study

2.3.1 Numerical analysis of long-term performance of monopile-supported offshore wind turbines:

Yang et al.(2017) presents a finite element model to examine the long-term performance of large diameter monopiles in sand. The model considered the impacts of long-term cyclic loading on the pile-soil interaction. The model's findings demonstrated that taking into account the effect of long-term cyclic loading on monopile's serviceability limit state causes noticeably larger deflection and rotation at pile. The programme ABAQUS was used to create a 3D FEM to study wind turbine-pile-soil system. Turbine, tower, blades, linkage section, tubular steel pile, dirt around pile, soil inside pile, and endless boundary elements were the model's eight key components. The influence of long-term cyclic loading was taken into account in one of two pile-soil interaction instances compared in the model, whereas it was omitted in the other. 3D rigid quadrilateral elements were used to model turbine, while brick elements were used to depict the earth. One-way infinite solid elements were used to simulate the infinite border elements. The earth was supposed to be an elastic-plastic medium, whereas the components were thought to be linear elastic.

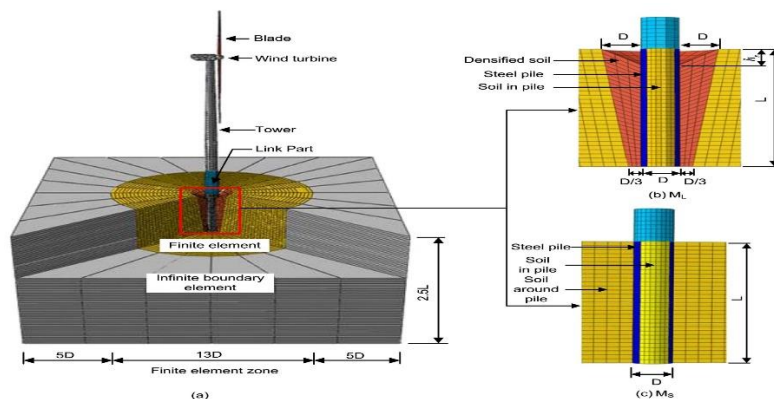


Figure 9: Three types of 3D FEM were built: (a) Entire model; (b) pile-soil interaction with consideration for long-term effects; and (c) pile-soil interaction without such considerations.

The pile-soil interface was modelled in the 3D FEM using ABAQUS's tiny sliding, surface-to-surface master/slave contact pair formulation. The dirt around and inside the pile was designated as the slave surface, while the pile's outside and inner surfaces were designated as the master surface. Kinematic restrictions in normal and tangential directions managed contact conditions between the two surfaces.

Using a powerful tension mechanism, four steel monopiles were tested under lateral loading circumstances. In this work, the 3D FEM for pile-soil interaction was validated using two of the test heaps. The test piles' specifics are displayed in figure 9. Sandstone, gravely sand, and other soil types

made up the soil profile. In sand layers above sandstone, both test piles were set up. Both the first and second monopiles required loading in five and three phases, respectively. At each stage, the pile head's displacement was measured. When test data and calculated results for pile head deflection were examined, it was found that there was good agreement between the two. This suggests that as lateral load increases, lateral displacement at pile head also increases.

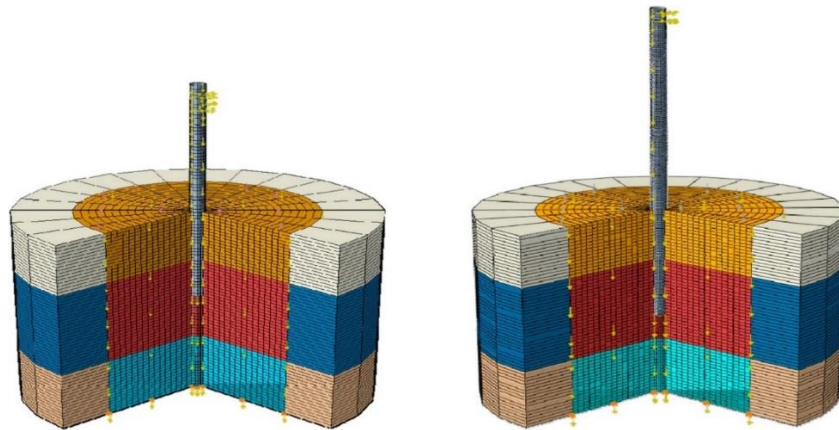


Figure 10: Mesh details (a) test pile 1; (b) test pile 2

The study's major findings indicate that, because long-term cyclic loading can greatly increase deflection and rotation at the pile head, it should be taken into account during design

2.3.2 Numerical simulation of Monopiles in Dense Sand:

Hawlder et al. (2016) evaluated the capability of monopiles to resist lateral stresses in thick sand using finite element models. The modified Mohr-Coulomb model, which incorporates pre-peak hardening, post-peak softening, as well as the impacts of mean effective stress and relative density, was used to investigate the stress-strain behaviour of thick sand. In comparison to the normal Mohr-Coulomb model, the modified Mohr-Coulomb model, according to the study, offered a superior simulation of the load-displacement behaviour shown in model testing. A monopile was set up in a lot of sand. In the simulation, the monopile is subjected to lateral stress at various eccentricities, or offsets, from the monopile's centre. The soil is modelled using C3D8R components and the simulation is run using the Abaqus programme. Pure moments, or rotating forces, imparted to the pile head are the only forces taken into account by the simulation. Modelled earth surrounds the monopile. Using a half-circular domain with dimensions of $15 D$ in diameter and $1.67 L$ in depth, with the top boundary being allowed to move and the bottom boundary being constrained from moving vertically. The lateral force and moment at the pile head are produced by applying a displacement or rotation at the reference point, which is positioned at a distance e above the pile head. The pile is modelled as a rigid body.

The study looked at how the stiffness of the pile, which is quantified by a metric called R , affects the interaction between a pile and soil. R is computed using the soil, the pile's Young's modulus, and its moment of inertia. The pile acts like a rigid body when its length (L) is approximately 1.48 times its radius (R). The pile behaves like a flexible body if L is approximately 4.44 times R . As is the norm with monopiles in offshore wind turbine foundations, the pile in this study was modelled as a rigid body to reduce computing time.

Four centrifuge experiments were performed using 18 m-long, 3-m-diameter monopiles in saturated, thick sand (90% relative density) in order to implement the MMC model using a user function written in FORTRAN. In the experiments, the eccentricities at which the lateral load was applied were 27.45 m, 31.5 m, 38.25 m, and 45.0 m.

With the exception of one test where the beginning stiffness was greater in the FE analysis, the FE analyses and centrifuge tests showed fair agreement. A rotation criteria was used to calculate the monopile's load-bearing capability, and the rotation of the pile was obtained by plotting the lateral displacement of the pile against depth. For significant eccentricities, the point of rotation was determined to be around $0.7 L$.

For provisional estimations of capacity, it was discovered that the streamlined model based on a linear pressure distribution proved useful. Based on empirical formulae, it was discovered that large-diameter monopiles have a larger capacity than small-diameter piles.

2.3.3 FEM of lateral loaded monopile in non-homogenous clay:

Using a 3D finite element model, Chen et al. (2009) examined the behaviour of large diameter monopile foundations in non-homogeneous clay under horizontal stress, including wind and wave loads. The link between horizontal displacement or rotational angle and the horizontal ultimate bearing capacity was looked at. A numerical 3D finite element model is used. For the study, it is assumed that the monopile foundation, which has a diameter of D and an embedment depth of L , is stiff and set into the ocean bottom. The border should be selected so that the effects of fictitious boundary conditions are eliminated. According to figure 12, h is the distance between sea level and the seafloor, and for the example scenario, a breadth of $8D$ and a depth of $5L$ are selected. It is presumed that the bucket foundation's density is the same as the soil around it. Twenty node brick pieces mimic the monopile foundation's structure as well as the soils within and outside of it.

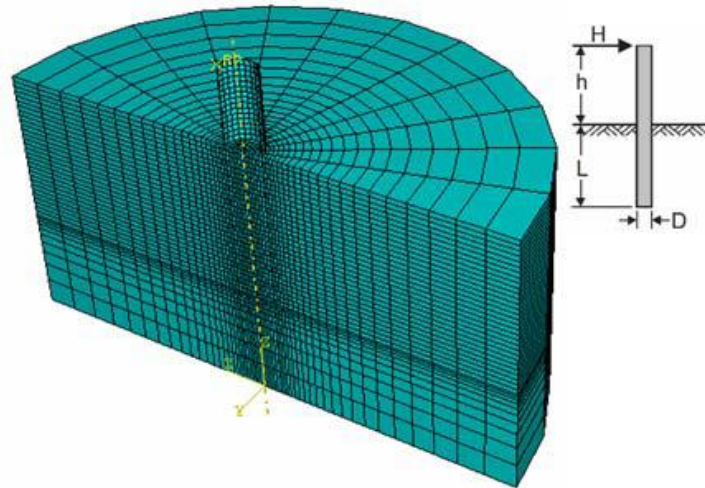


Figure 11: FEM of Pile

The model takes into account the effects of the foundation's stiffness and the state of the soil. The Young's modulus of the soil is assumed to vary linearly with depth while keeping a fixed modulus ratio, and the model employs a Mohr-Coulomb failure criteria to calculate the undrained material response of the soil. Given that the bucket foundation has a young's modulus of 2.1×10^5 MPa and a poisson's ratio of 0.125, it is anticipated that it will act elastically. The idea of "local support" nodes is used in the model to allow for rough contact between the footing and foundation soil, and the friction coefficient between the master and slave surfaces is set at 0.5 as illustrated in figure 13

The horizontal ultimate bearing capacity of a monopile foundation in non-homogeneous clay soil exposed to horizontal loads was assessed using a finite element analysis. The monopile foundation is taken into account as stiff, and the soil is modelled using an elasto-perfectly-plastic constitutive model based on the Mohr-Coulomb failure criterion. The ultimate bearing capacity is calculated by the point at which the slope of the load-displacement curve approaches zero, signifying the soil has achieved its limit equilibrium condition. The load is supplied using a displacement-controlled technique. Investigation is done into how the soil characteristics and horizontal loads affect the final bearing capacity of the monopile foundation.

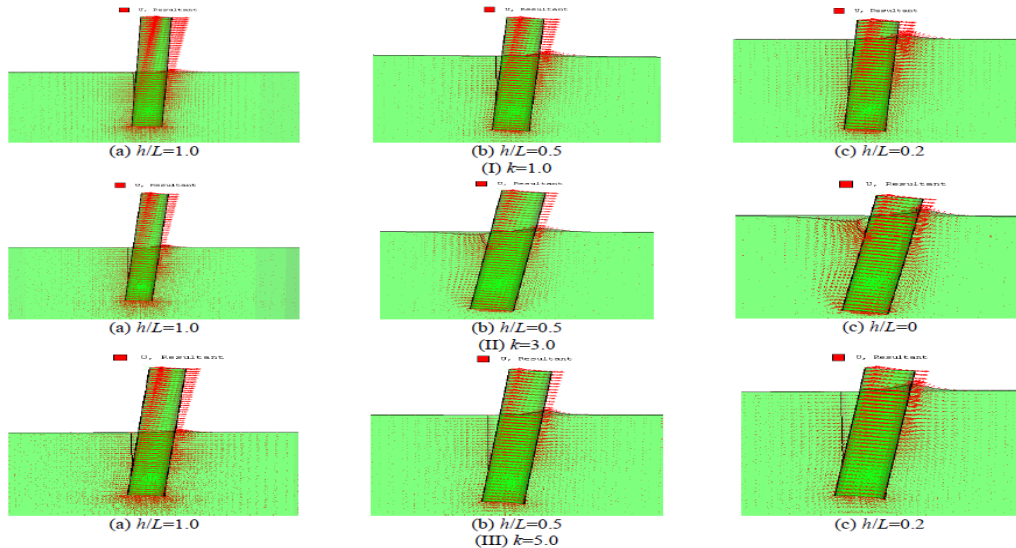


Figure 12: Failure Mechanism of Monopile Foundation

After thorough investigation and study, it was concluded that:

- The convex shaped distribution of deformation was initiated at bottom of the bucket foundation following application of lateral loads. In the direction of loading as well as the opposite direction, the sidewalls of the monopile foundation formed a significant passive wedge and a minor active zone, respectively. Due to an increase in soil strength with a higher L/D ratio, the failure mode was minimized.
- On non-homogeneous clay, the lateral ultimate bearing capacity of the monopile was improved by f .
- Using the ratio of h/L , horizontal stiffness and moment stiffness may be used to calculate the ultimate horizontal bearing capacity of a monopile.

2.4 Experimental Study

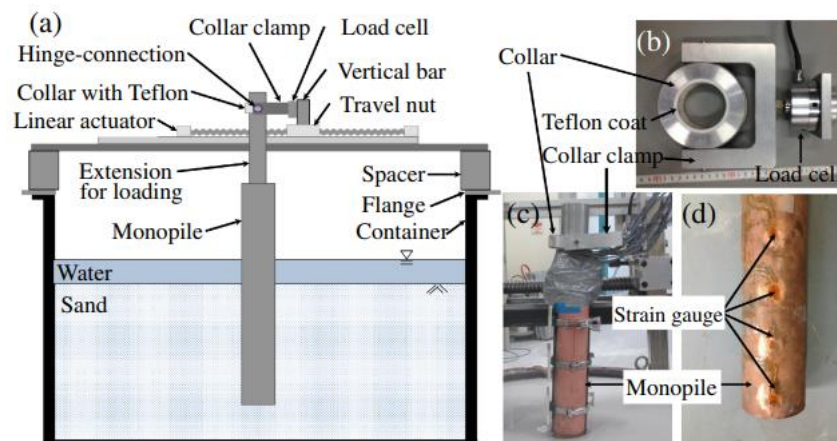
2.4.1 Experimental generation of p-y curves for Large-Diameter Monopiles in Sands:

Centrifuge Tests

Choop et al. (2016) illustrates the creation of experimental p-y relationships for monopiles in thick sands using centrifuge test findings that revealed softer monopile behavior than what the API and predicted Reese techniques. Impact of socketing a pile's tip in rock-bearing layers was also Investigated. As the depth approaches the much stiffer and stronger rock-bearing layer, it is shown that early slope of the p-y relationships in dense sand layers grow significantly stiffer. It was determined that the generated experimental p-y relationships foresee the responses of large-diameter monopiles since the lateral load-displacement curves were found to be well matched with the measured lateral load displacement curves. A centrifuge model of monopiles that were subjected to horizontal loads and moments made up the experimental in this investigation. The equipment of the

Korea Advanced Institute of Science and Technology, a 5 m radius beam model, was used for the experimentation. The centrifuge assembly can withstand 240g-ton. Kim et al. (2013). have shown more information about the centrifuge. Both 60g and 75g of centrifugal acceleration were used throughout the centrifuge tests. In a study, steel, cylindrical container, soil samples were prepared. The container was 900 mm in diameter and 700 mm high internally, simulating a test bed model with dimensions of up to 54 m in diameter by 42 m in depth at 60 g and 67.5 m in diameter by 52.5 m in depth at 75 g. Two model piles made of steel and copper were used in the tests. To evaluate various flexural stiffness (EI) or pile t/D ratios, two distinct types of materials were mostly utilised. Tests M1–M3 were carried out on a single layer of sand that was thick ($D_r = 82\text{--}86\%$). The piles were inserted between 5.2 and 7.1D. The pile was embedded in sand for the fourth test (M4), with the bottom 1.8D immersed in a layer of rock.

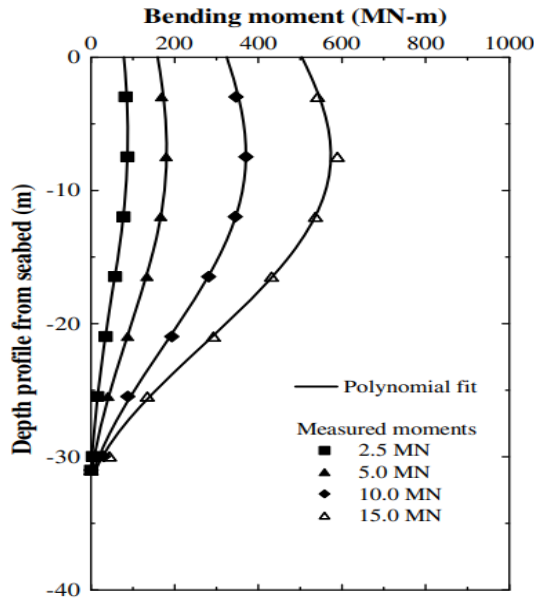
By employing an automated sand-raining mechanism, the air pluviation method was used to produce the sand layers. By adjusting the size of sieve holes and the height from which the sand particles were dropped, it was possible to regulate the relative density of the sand. A lateral load and a moment were applied on monopile using a linear actuator with respect to the level of the seafloor. The loading system is depicted in Figure 14. A travel nut on the linear actuator linked to and lateral loaded the monopile, as shown in figure 15



(a) Schematic diagram; (b) photograph of the clamping system; (c) photograph of the assembly of the monopile-linear actuator system; (d) photograph of a monopile with strain gauges

Figure 13: Schematic diagram of centrifuge test

The deformation measurements down the pile shaft yielded the bending moment distributions at the depth of the monopiles Figure 2.16 shows the distributions of the bending moments from test M1 for four distinct lateral loads, which are 2.5, 5.0, 10.0, and 15.0 MN.



Bending moment distributions measured by strain gauges in test M1

Figure 14: Bending moment distribution

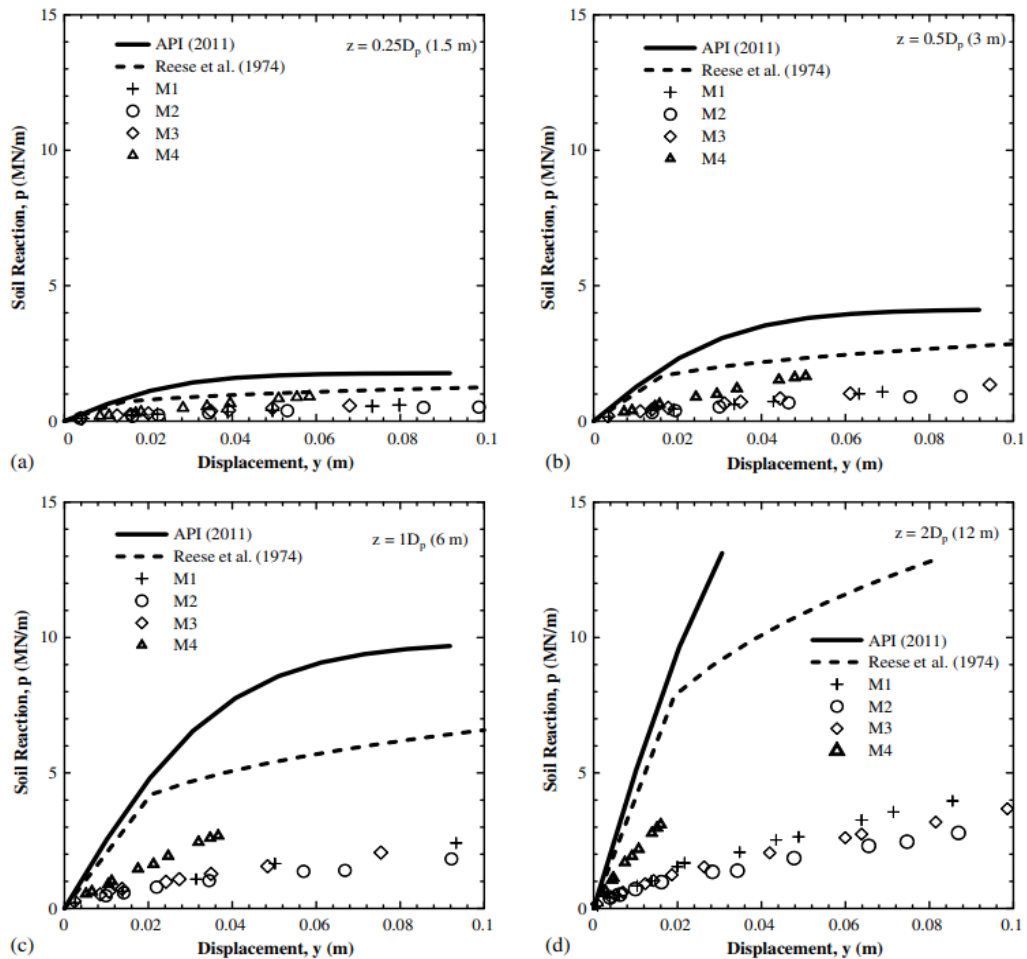
These moments were taken into account to develop the experimental p - y curves. The moment distributions were expressed mathematically to obtain the soil reaction and lateral displacement along the monopile and generate the experimental p y curves. The soil reaction and displacement were obtained by the following equations (2.1,2.2):

$$y = \int(\int \Phi dz) dz = \int(\int \frac{M}{EI} dz) dz \text{-----}(2.1)$$

$$p = -\frac{d^2M}{dz^2} \text{-----}(2.2)$$

Figure 17 demonstrates how, for a given kind of soil, the p - y relationship stiffens with increasing depth. It has been demonstrated through comparison of the findings from tests M1 and M2 and M1 and M3 that the embedded length and stiffness conditions had little bearing on the lateral behaviour of the monopiles. The experimental p - y relationship is stiffer in the presence of a rock bearing layer than it is in the absence of one, according to a comparison of the lateral monopile behaviour between

the case of tests M1–M3 and that of test M4. The pile's p-y connection in the comparatively weak layer next to the stiffer layer is controlled by the considerably stiffer layer. Yang and Jeremic have also recognised this effect of strong and stiff layers on the p-y relationship of a neighbouring comparatively weak layer. (2005) on the findings of a thorough 3D FEM investigation.



Comparison between experimental p - y data points and the Reese and API p - y relationships ($\gamma' = 9.54 \text{ kN/m}^3$ and $\phi = 42^\circ$) for various depths z : (a) $z \cong 0.25D_p$ (1.5 m); (b) $z \cong 0.5D_p$ (3.0 m); (c) $z \cong 1.0D_p$ (6 m); (d) $z \cong 2.0D_p$ (12 m)

Figure 15: Comparison between experimental p - y data points and the Reese and the API p - y curves. Nonlinear soil springs are made to find the behavior of a monopile subjected to horizontal loading. The nonlinear characteristics of the springs can be represented by the following hyperbolic function (2.3) (Georgiadis et al. 1992; Liang et al. 2009):

$$p = \frac{y}{\frac{1}{K_t} + \frac{y}{pu}} \quad \text{-----(2.3)}$$

Eq. (3) is used to express stress-strain relationships in soil problems (Kondner 1963). From the results presented in figure 17, Due to the loading system's flaws, it is challenging to determine the peak soil

response at each level; as a result, the experimental data was fitted to Equation using the p_u equation supplied by the API technique. (3). The ultimate soil resistance values were assumed as those proposed by API (2011). This supposition was crucial because the lateral loading system's limitations prevented the p_u values from being determined experimentally. As a result, here is how the effect of the p_u values on monopile behaviour is investigated. It was determined that in the absence of lateral displacements (or lateral loads), the ultimate soil resistance had no bearing. The effect of an extremely stiff layer on the topological interactions of weak layers was another intriguing experimental finding of this study. It was discovered that the presence of hard rock layers had a significant impact on the initial stiffnesses of the p - y relationships at different depths.

2.5 Properties of Sand at seabed of Pakistan

In recent years, with the increasing demand for offshore wind energy, there has been a growing interest in the study of the technical and physical properties of seabed sand in coastal areas of Pakistan. Several studies have been conducted to investigate the geotechnical properties of the seabed sand, which play a critical role in the design and installation of offshore wind turbines.

One of the earliest studies on the geotechnical properties of the seabed sand in Pakistan was conducted by Hussain and Tariq (2008). They analyzed the grain size distribution, specific gravity, and permeability of the sand samples collected from the coast of Karachi. Their results showed that the seabed sand was predominantly medium-grained, with a specific gravity ranging from 2.63 to 2.67, and a permeability of 0.0018 cm/s. The study also found that the angle of internal friction of the sand was approximately 33° .

Another study conducted by Ali et al. (2011) investigated the shear strength characteristics of seabed sand in Karachi Harbor. The researchers conducted a series of laboratory tests, including direct shear tests, unconsolidated-undrained triaxial tests, and consolidation tests, to find the shear strength of the sand. The results showed that the seabed sand had a friction angle of 32.5° and a cohesion intercept of 17.5 kPa.

In a more recent study, Ansari et al. (2018) analyzed the geotechnical properties of seabed sand at the Gwadar Port, located on the southwestern coast of Pakistan. The researchers conducted a series of laboratory tests, including grain size analysis, Atterberg limits tests, and direct shear tests, to determine the geotechnical properties of the sand. The results showed that the seabed sand had a median grain size of 0.29 mm, a liquid limit of 31%, and a plastic limit of 18%. The direct shear tests revealed that the sand had an average friction angle of 34.3° and a cohesion intercept of 0.26 kPa.

Another important property of seabed sand is its dynamic behavior under wave loading. Khalid et al. (2017) conducted a study to investigate the dynamic response of seabed sand in Karachi Harbor. The researchers used a series of small-scale physical model tests to determine the acceleration and pore pressure distribution in the seabed sand due to wave loading. The results showed that the seabed sand exhibited significant liquefaction and settlement under wave loading, which could have significant implications for the design and stability of OWTs.

In addition to the studies mentioned above, several other studies have been conducted on the geotechnical properties of seabed sand in coastal areas of Pakistan, including studies on the bearing capacity of sand, the influence of sediment characteristics on soil strength, and the impact of sediment disturbance on seabed stability. Overall, these studies provide valuable insights into the technical and physical properties of seabed sand in coastal areas of Pakistan, which can be used to design the offshore wind turbines.

Methodology

3.1 General

A non-linear three-dimensional numerical-based design approach was used to design the laterally loaded offshore monopile foundation in the coastal regions of Pakistan. For this purpose, a parametric study was performed in which the configuration of pile, loading conditions, and soil properties were varied. Several 3D finite element models were constructed and analyzed in this study using the finite element analysis software ABAQUS (ABAQUS-2017).

3.2 Finite Element Model Parts:

The finite element model consisted of two parts:

- Pile.
- Soil.

3.2.1 Pile Modelling:

The parametric study utilized 3 piles of 3m, 5m, 7m of diameter and having a constant embedded length (L) of 30 m. The non-dimensional ratio (L/D) of the monopiles was between 4.28 to 10. The thickness (*tp*) of the piles was 0.025 m.

The geometry of the monopiles used in the study is given in [Table 1](#). The pile was modeled as a linear elastic, solid element in the ABAQUS. In real-life monopile is a hollow structure therefore the elastic modulus (*E_s*) of the monopile was adjusted from 200 Gpa to a value to specific value using the relationship between elastic modulus and moment of inertia (*I*) of piles which given as:

$$E_{solid}I_{solid} = E_{hollow}I_{hollow} \text{ ----- (3.1)}$$

The pile had a density of 7850 Kg/m³ and a Poisson's ratio of 0.3. The pile was discretized by C3D8R Hexahedral brick elements.

The FEM mesh for the pile was generated from using the seed edges techniques which helps in controlling the number of mesh elements of a part. The number of FEM mesh elements and nodes is given in table 2.

Table 1: Pile geometries

Pile reference	Diameter (m)	Embedded Length (m)	Thickness (mm)	L/D	Adjusted Elastic Modulus (Pa)
P1	3	30	0.025	10	1.30E+10
P2	5	30	0.025	6	7822783763
P3	7	30	0.025	4.285	5599920697

3.2.2 Soil Modelling:

Two soil profile resembling the Offshore soil condition of Pakistan was selected. The profile mostly consisted of sand and is shown in Table 2. The depth of the soil was taken as 40 meters in accordance with the soil profile and the length and width of the profile are 10D and 20D respectively for different measures of diameter, to create its model in ABAQUS. The elastic-perfectly plastic Mohr-coulomb constitutive model was used to model the behavior of sand. This model characterized the following parameters:

- Young's modulus (Es).
- Angle of internal friction (Φ).
- Poisson's ratio. (ν)
- Angle of dilatancy. (ψ)
- Cohesion

Utilizing the parametric study Three Different angles of friction were assumed which are 30, 35, and 40 degrees. Table 2 shows the value of the above-given parameters for the internal angle of friction at 30 degrees. The value of young's modulus (Es) was reversed calculated from the angle of internal friction (Φ). To measure the young's modulus of the sand the SPT-N values were used. First the SPT- $(N_1)_{60}$ values from the Hatanaka and Uchida empirical relation

$$\Phi' = \sqrt{20(N_1)_{60} + 20} \text{-----}(3.2)$$

The values obtained from this equation were further converted to $(N)_{60}$ values using another empirical relationship

$$(N_1)_{60} = (N)_{60} \sqrt{\frac{101.325}{\sigma}} \text{-----(3.3)}$$

Where,

σ is the value of effective vertical stress.

To calculate the Elastic Modulus of the sand J. E. Bowles' empirical relations for the normally consolidated soil were used.

$$E_s = 6000N_{60} \text{-----(3.4)}$$

The angle of dilation (ψ) was calculated using the given relation which is true for non-cohesive soils as in this study:

$$\psi = \Phi - 30 \text{-----(3.5)}$$

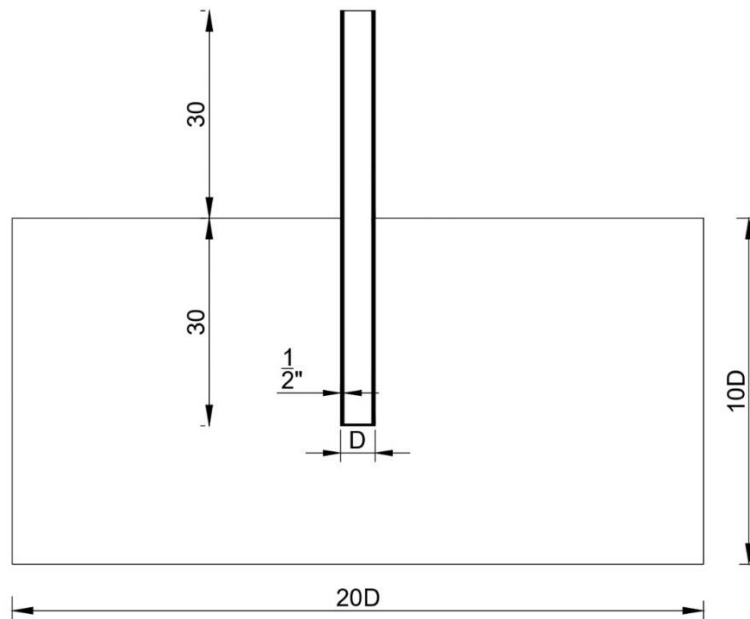


Figure 16: Monopile schematic and parametrized diagram for dimensions

FE-mesh was formed using the same technique as the of pile the number of FE-mesh are shown in table 3.

Table 2: Soil profile and soil parameters used for FE-modelling for $\Phi=30$ degree

Total Depth(m)=40	
Depth(m)	Description
0-6.0	Grey silty fine sand
6.0-11.50	Grey fine sandy silt with trace mica, and little organic matter
11.50-17.50	Grey silty sand and seashell, trace mica
17.50-20.50	Greyish green silty clay, low plasticity
20.5-25.20	Greyish green clayey silt, low plasticity
25.20-31.0	Greyish green, weak to moderately weak, friable sandstone, fine-grained, fractured
31.0-40.0	Greyish green, weak to moderately weak, friable sandstone, fine-grained, fractured

Table 3: Soil parameters used for FE-modelling

Soil Parameters	Numerical Values
Angle of Internal Friction	30°, 35°,40°
Unit Weight of soil	18.5 KN/m ²
Poisson's ratio	0.25
Angle of dilatancy	0°
Cohesion	0 KN/m ²

3.2.3 FE-Mesh:

The mesh was created such that areas of soil close to the pile had a finer mesh, while those elements of soil away from the pile have coarser mesh to achieve more accuracy in desired results and to decrease the time of analysis thus making it a more efficient approach. The number of elements of pile and soil is given in table 2 and table 3

3.2.4 Pile-soil interaction:

Surface-to-surface master/slave contact pair formulation was used to represent the soil-pile interface. Because the pile is substantially stronger than the earth, the soil that comes into touch with the pile was designated the slave surface. The penalty friction technique, which takes into consideration a fundamental Coulomb friction model and permits modest amount of elastic slip, was used to manage the tangential behaviour. The value of coefficient friction (μ) was found using the following equation:

$$\mu = \tan\left(\frac{2}{3}\Phi\right) \text{-----(3.6)}$$

Here,

Φ is the angle of internal friction.

A Tie constraint was used at the bottom of the pile. In which the pile was modeled as the master and the soil in contact was modeled as the slave surface.

3.2.5 Boundary Conditions:

The x- and y-directional movement of the nodes on the soil perimeter was restricted. The whole soil's base was exposed restrained in all three directions by using the Pin-connection, while the on faces in the x and y direction were restrained using the roller support condition. Figure 18 shows the boundary conditions applied to the model.

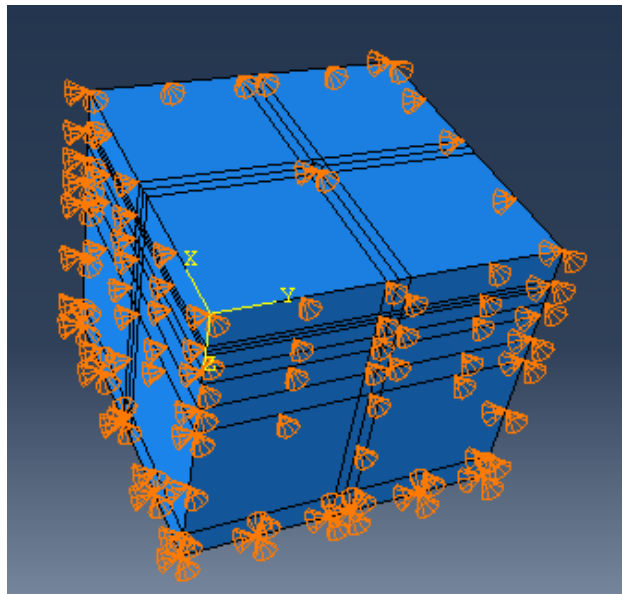


Figure 17: Boundary Conditions

3.2.6 Loading:

Two types of loads were used in the analysis which includes weight of pile and soil and the lateral loading due to the waves and wind. The weight was applied by applying a gravity force equal to 9.81 m/s^2 and lateral load was applied in the form of concentrated force acting on the monopile. Table 4 shows the lateral load applied on the monopile.

Table 4: load applied

Sr.no	Load (MN)
1	2.5
2	5
3	10
4	15
5	20

3.2.7 Steps:

The analysis was run in three steps. For all simulations static, general procedure was used.

Step-1: In step 1 the gravity force was applied to the soil to incorporate the impact of weight of soil in the analysis as shown in [Figure 19a](#). The time duration of this step was 1 second. During this step there was no interaction created and only gravity acted on the soil.

Step-2: In this step, the gravity force was applied on the on pile as shown in [Figure 19b](#). the interactions were created in this step. The time duration of this step was 1 second.

Step-3: During this step the lateral load was applied on the pile. This is the step in which actual deformation of soil begins to take place and tangible results are obtained after this step. The time duration of this step was 1 second. [Figure 19c](#) shows this step.

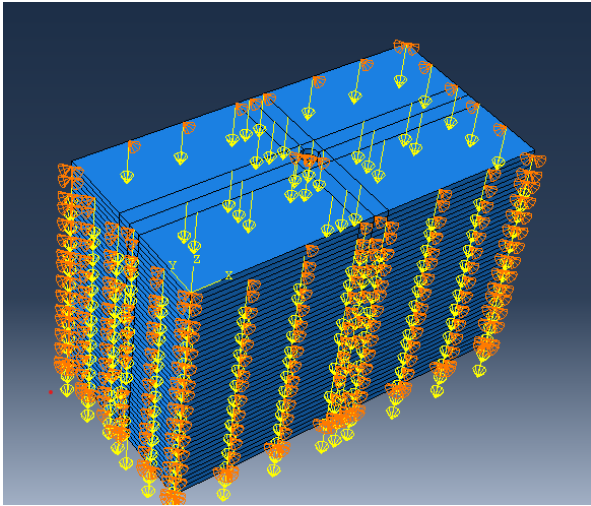


Figure 18(a): Step-1

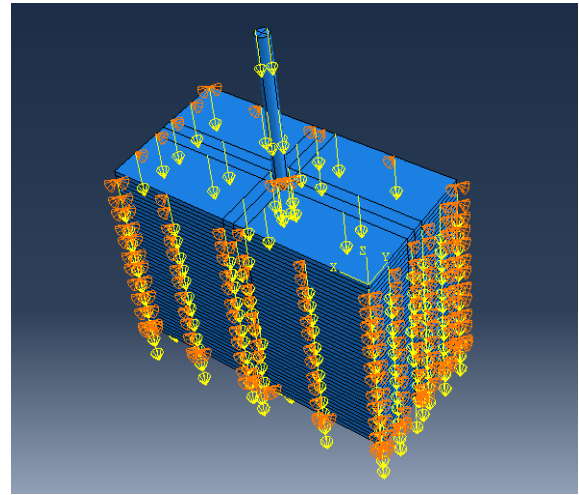


Figure 18(b): Step-2

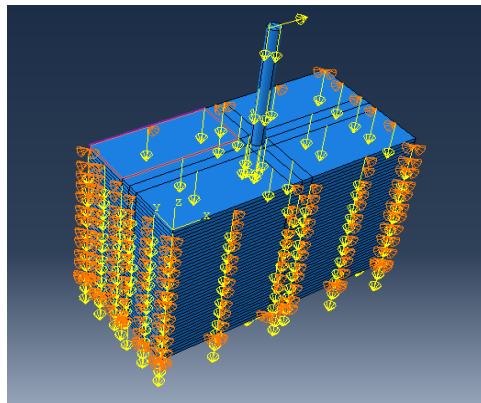


Figure 18(c): Step-3

Figure 18: Abaqus Modelling steps

The results and the comparison drawn between present study and previous is described in up coming section.

3.3 Statistical Analysis:

As a result of non-linear three-dimensional numerical-based analysis of ABAQUS, the P - Y curves were generated upon which several statistical approaches were used to determine the curve of best fit. For this purpose, a detailed analysis was performed using the ORIGINPRO Software. Origin Pro is a widely used data analysis and graphing tool. Its major functions include tasks such as data visualization, statistical analysis, curve fitting, and programming. OriginPro generally used the non-linear least square method to find the curve of best fit for the given curve. This method reduces the sum of squared differences between the observed data points and the values predicted by fitting

function. It iteratively control the parameters of the chosen function until the best-fit line is obtained. Following procedure is adopted to find the equation of curve of a best fit:

- a) The p-y curve data, consisting of deflection (independent variable) and soil resistance (dependent variable), was taken into OriginPro.
- b) A scatter plot was generated to visualize the data points and their distribution.
- c) The "Analysis" menu was accessed to perform statistical analysis.
- d) The "Nonlinear Curve Fit" option was selected from the "Analysis" menu to fit a mathematical function to the scatter plot.
- e) In the curve fitting menu, the fitting function was selected which was thought to be captured by the curve.
- f) Initial parameters were adjusted.
- g) After the fitting process, OriginPro provided the equation of the best fit, along with statistical information. This included the coefficient of determination (R-squared), which indicates the proportion of the variability in the dependent variable explained by independent variable. A higher R-squared value (closer to 1) indicates a better fit.
- h) OriginPro also provided standard errors of the fitted parameters. These standard errors represent the uncertainty or variability in the estimated parameter values and can be used to assess the statistical significance of the parameters.
- i) The best-fit curve was overlaid on the plot of the p-y curve data. This allowed for a visual assessment of the fit quality and a comparison with the original data points.
- j) The statistical significance and goodness of fit were evaluated using the R-squared value. A higher R-squared value indicated a greater amount of variability in the dependent variable explained by the independent variable. Additionally, smaller p-values suggested that the fitted parameters were statistically significant.
- k) The equation of the best fit was interpreted to understand the mathematical relationship between deflection and soil resistance in the p-y curves. The value of parameter "a" represented the scaling factor or the initial value of the soil resistance, while the parameter "b" determined the rate of change of the soil resistance with respect to deflection.

The results obtained from the curve fitting analysis are documented in the subsequent sections, including the equation of the best fit, the values of the fitted parameters, their standard errors, the R-squared value, and any other relevant statistical information. These findings provide valuable insights into the behavior of the p-y curves and can be used for further analysis and design purposes.

Results

4.1 FEM Analysis of 3m diameter:

4.1.1 General Properties

The soil profile considered for this parametric study was sand consisting of 40 layers each layer with a thickness of 1 meter. With the Mohr-Coulomb failure criteria, the sand was modelled as an elastic perfectly plastic material

The coefficient of friction for the pile-soil interface (μ) was set to 0.4. The elastic modulus of soil varied from 9.064 MPa for the first layer to 80.56 MPa for the last layer because of the impact of overburden pressure.

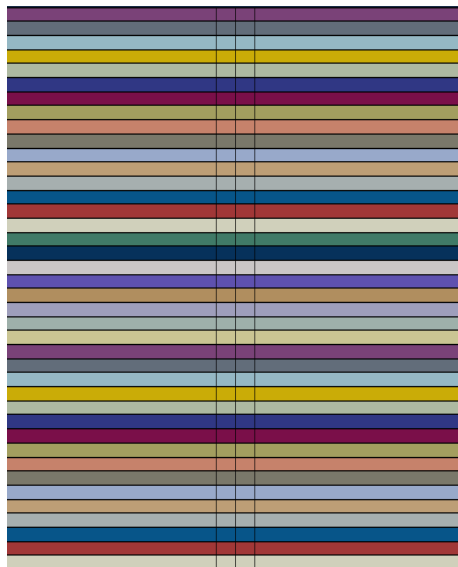


Figure 19: The 40 layers of the soil from top to bottom with increasing elastic modulus.

The structural properties of the pile are given in the table 5 below:

Table 5: Properties of pile

Pile Structural Element	Values
Diameter	3 meters
Total length	60 meters
Embedded length	30 meters

L/D ratio	10
Elastic Modulus	13 GPa

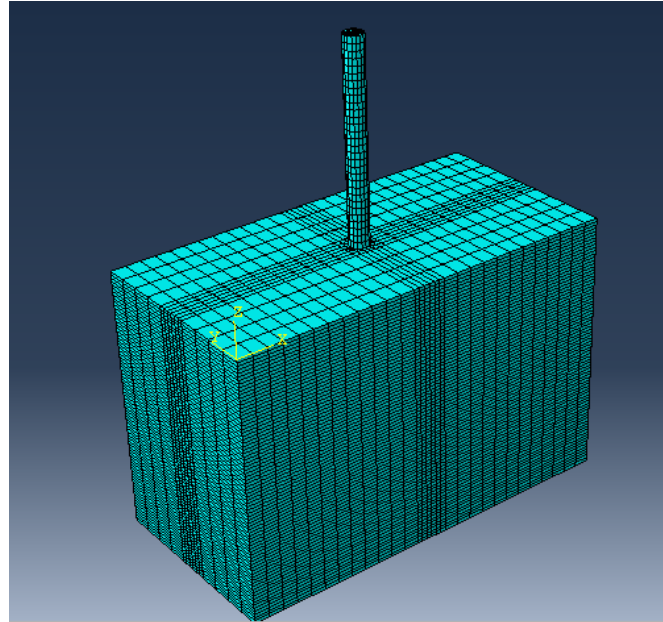


Figure 20: FEM Mesh

The FEM mesh elements used in this study for soil and pile are C3D8R Hexahedral brick elements with reduced integration. The details of mesh are given in table 6

Table 6: Detail of Mesh

Element	Element Type	Number of elements	Number of nodes
Pile	C3D8R	1920	38715
Soil	C3D8R	34200	2501
Total		36120	41216

4.1.2 Relationship between Depth and Bending Moment

For the FEA performed, the graphs between depth and bending Moment for the angle of internal friction 30° are shown in subsequent figures.

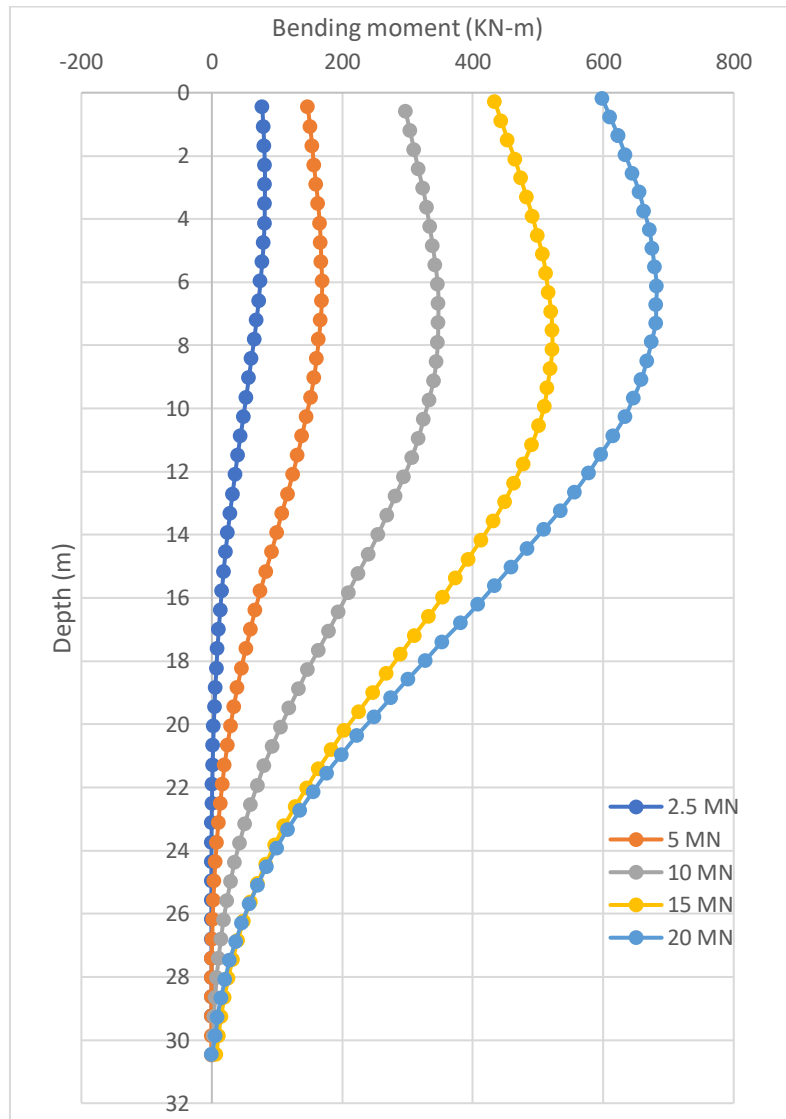


Figure 21: shows the relationship between Depth and Bending Moment for the angle of internal friction 30°

For the FEA performed, the graphs between Depth and Bending Moment for the angle of internal friction 35° are shown in the subsequent figures.

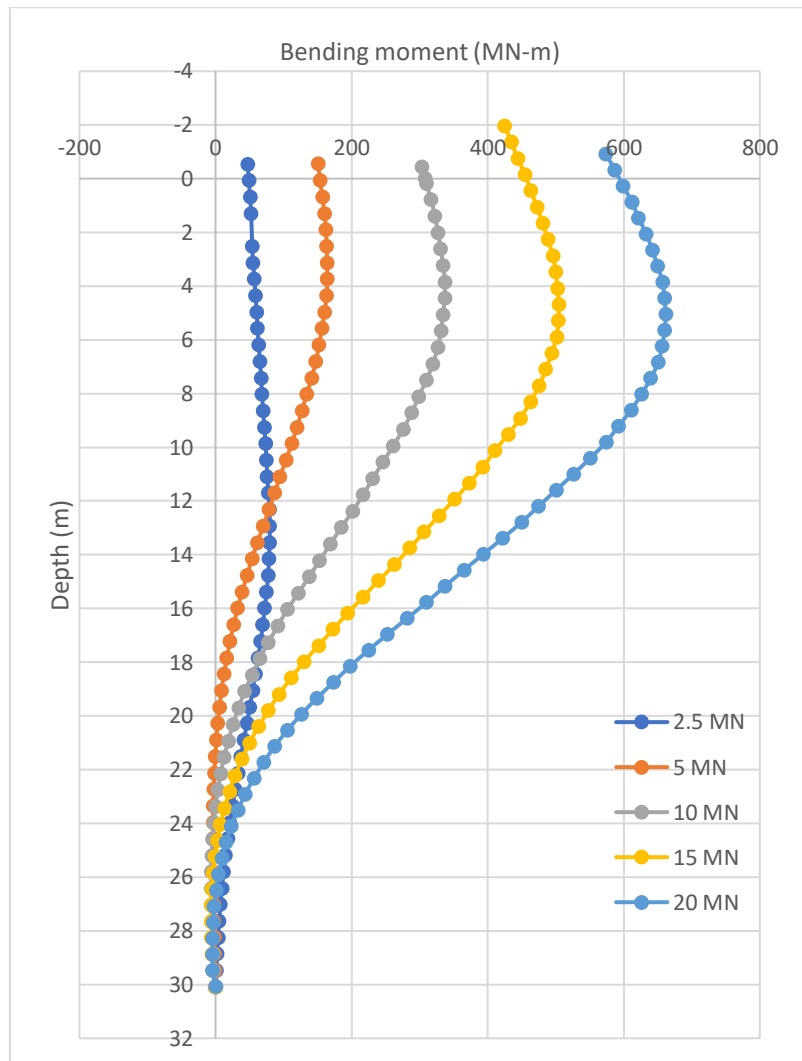


Figure 22: The relationship between Depth and Bending Moment for the angle of internal friction 35°

For the FEA performed, the graphs between Depth and Bending Moment for the angle of internal friction 40° are shown in the subsequent figures.

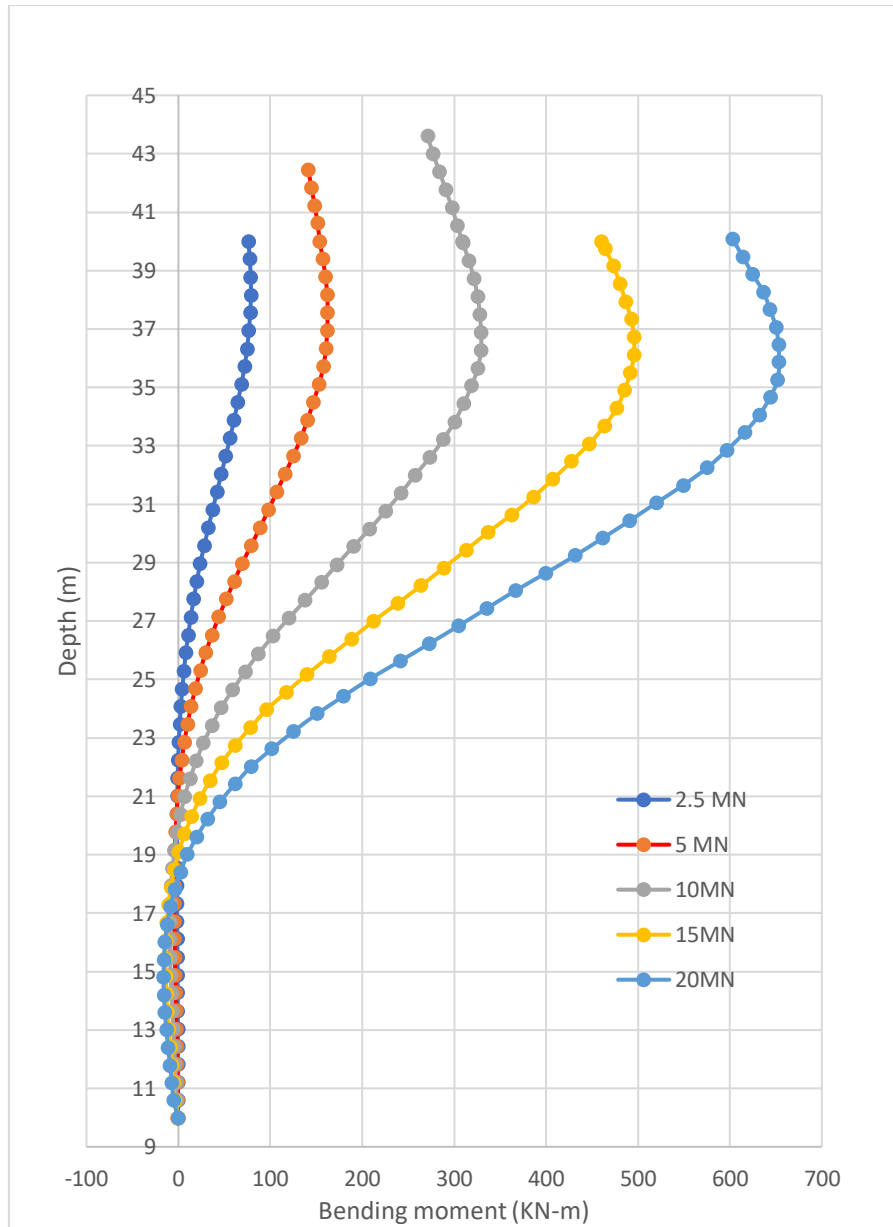


Figure 23: The relationship between depth and bending Moment for the angle of internal friction 40°

4.1.3 Relationship between depth and displacement

The relationship between depth and displacement in monopile design relates to the manner in which the movement or displacement of the monopile changes as embedment depth increases. Numerous elements, such as the soil's characteristics, the loads that are applied, and the pile design, can affect how far a monopile is displaced. The displacement typically tends to diminish when the monopile is buried deeper in the earth. This is due to the increased soil volume provided by the deeper embedment, which can withstand the lateral and vertical stresses occurring on the monopile. The soil's bearing capacity is increased with deeper embedment, reducing lateral and vertical displacements.

It's important to remember that depth and displacement are not necessarily related in a linear fashion. It may differ based on elements like the kind of soil, the size of the pile, the loads that are applied, and the installation techniques. In some circumstances, there can be a depth beyond which the displacement becomes minimal or becomes relatively constant. For the FEA performed, the graphs between the depth and displacement for the angle of internal friction 30° are shown in the subsequent figures.

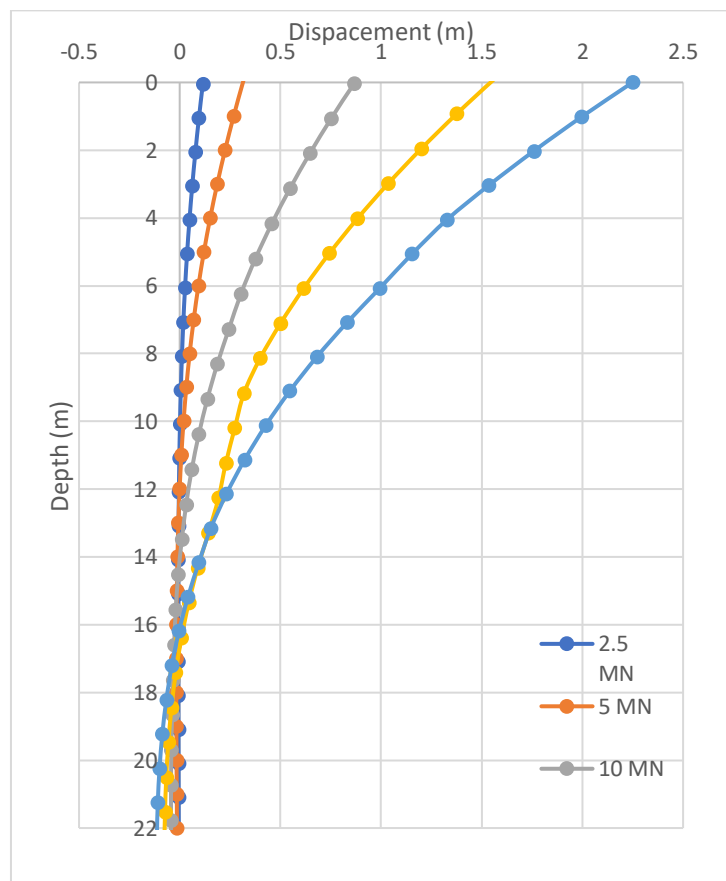


Figure 24: The relationship between depth and displacement for the angle of internal friction 30°

For the FEA performed, the graphs between the depth and displacement for the angle of internal friction 35° are shown in the subsequent figures.

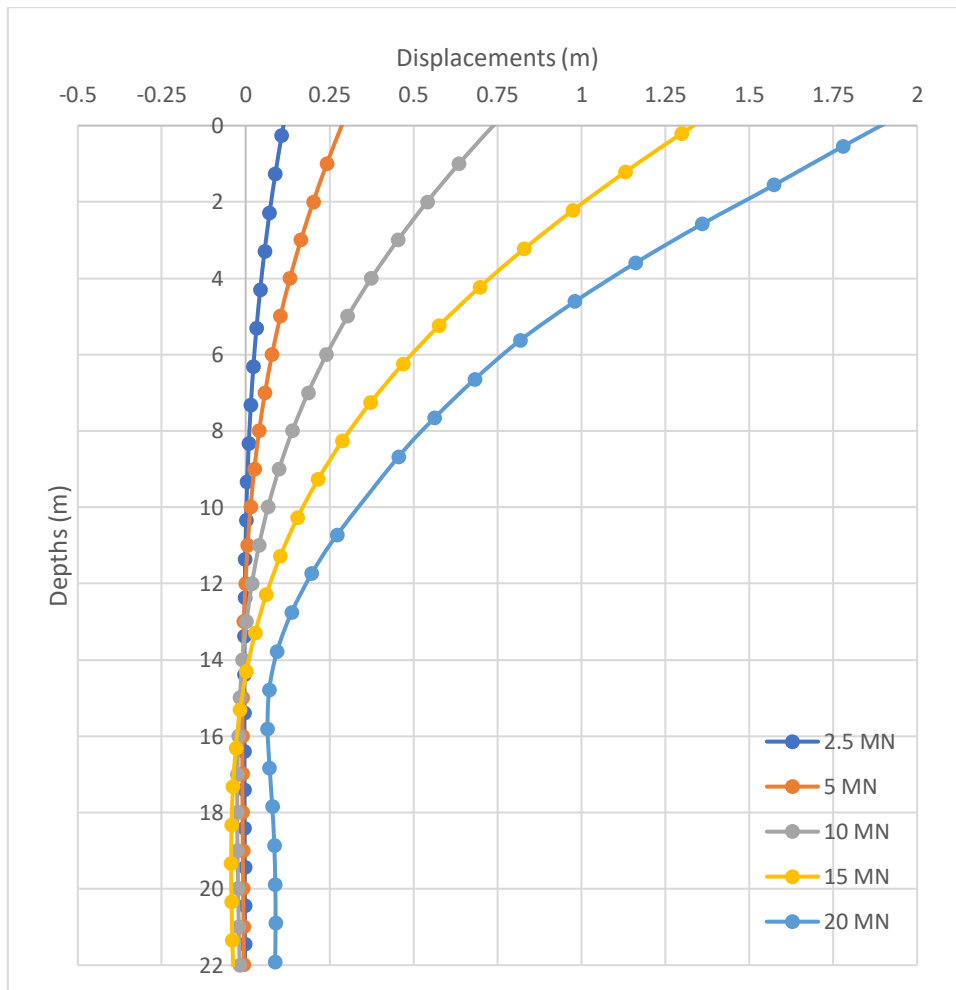


Figure 25: The relationship between depth and displacement for the angle of internal friction 35°

For the FEA performed, the graphs between the depth and displacement for the angle of internal friction 40° are shown in the subsequent figures.

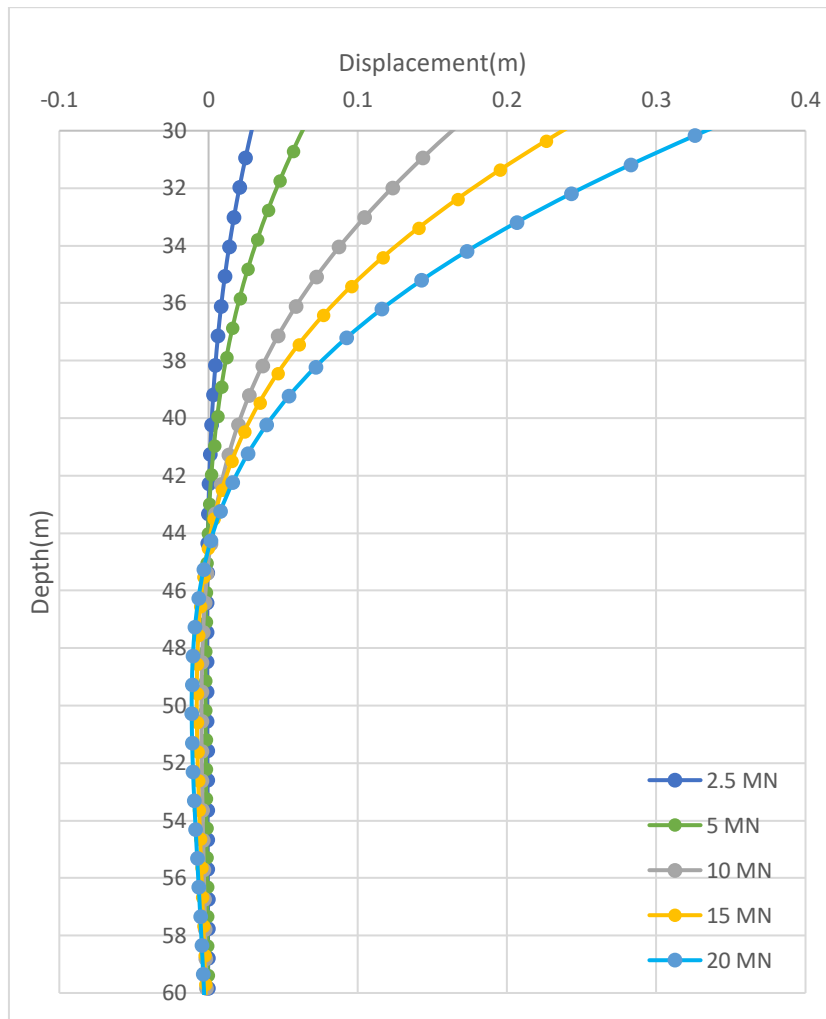


Figure 26: The relationship between depth and displacement for the angle of internal friction 40°

4.1.4 P-Y Curves

P-Y curves, which describe the lateral reaction of the pile under horizontal stress, are critical in the design of monopiles for offshore projects. They offer a way to simulate the interaction between the soil and the pile and calculate the monopile's lateral capacity. P-Y curves are often created using either numerical calculations or field experiments. The method of numerical analysis has been employed in this study. P-Y curves are generated in numerical simulations by simulating the soil around the monopile. To accurately depict the interaction between the soil and the pile, the soil's characteristics, including stiffness, strength, and nonlinear behaviour, are taken into account. The obtained pile deflections and soil responses are utilised to construct the P-Y curves after applying lateral loads to

the numerical model. Once obtained, P-Y curves are used in the design phase to evaluate the monopile's structural behaviour. By considering the lateral loads and anticipated soil conditions, we may assess variables like pile length, diameter, and wall thickness. We can estimate the maximum permitted loads, evaluate the pile's lateral stability, and optimize the monopile design to ensure its structural integrity and performance in offshore conditions by including the P-Y curves into structural analysis.

For the FEA performed, the P-Y curves for the angle of internal friction 30° are shown in the subsequent figures.

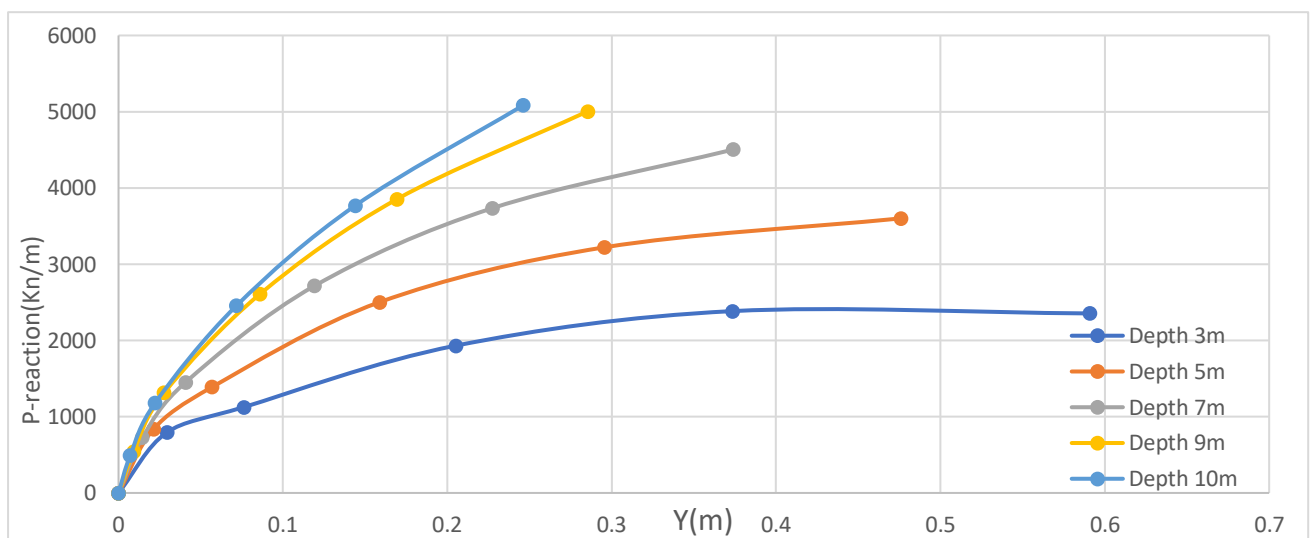


Figure 27: The P-Y Curves for the angle of internal friction 30°

For the FEA performed, the P-Y curves for the angle of internal friction 35° are shown in the subsequent figures.

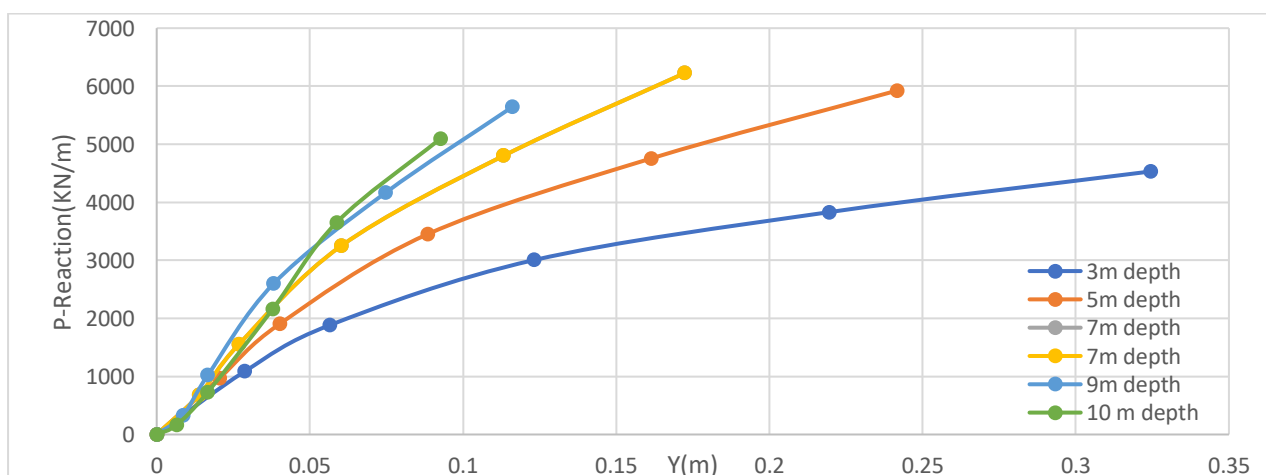


Figure 28: The P-Y Curves at (a) 2.5 MN load (b) 5 MN load (c) 10 MN load (d) 15 MN Load (e) 20 MN load for the angle of internal friction 35°

For the FEA performed, the P - Y curves for the angle of internal friction 40° are shown in the subsequent figures.

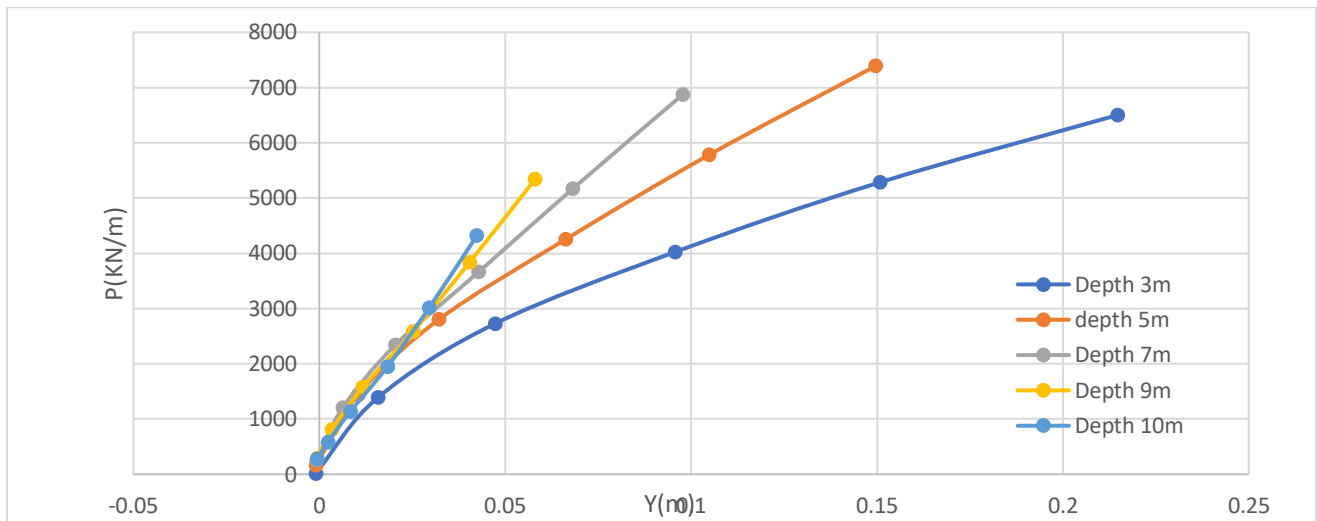


Figure 29: The P - Y Curves for the angle of internal friction 40°

As the depth increases, the P - Y curves are becoming more linear, indicating that lateral loads have much less impact at greater depths than the near-ground surface. Therefore P - y curves for depths of 3, 5 and 7 meters where P -reaction is maximum for the lateral load of 2.5, 10 and 15 MN are more critical for the design consideration of monopile with a diameter of 3 meters in given soil and loading conditions.

4.2 FEM Analysis of 5m diameter:

4.2.1 General Properties

The soil profile considered for this parametric study was sand consisting of 40 layers each layer with a thickness of 1 meter. The sand was modeled as an elastic perfectly plastic material with Mohr-Coulomb failure criterion.

The coefficient of friction for the pile-soil interface (μ) was set to 0.4. The elastic modulus of soil varied from 9.064 MPa for the first layer to 80.56 MPa for the last layer because of the impact of overburden pressure.

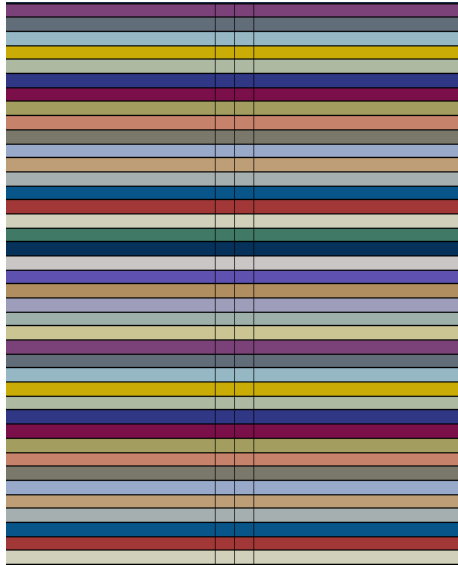


Figure 30: The 40 layers of the soil from top to bottom with increasing elastic modulus

The structural properties of the pile are given in the table below:

Table 7: Pile properties

Pile Structural Element	Values
Diameter	7 meters
Total length	60 meters
Embedded length	30 meters
L/D ratio	8.57
Elastic Modulus	7.82 GPa

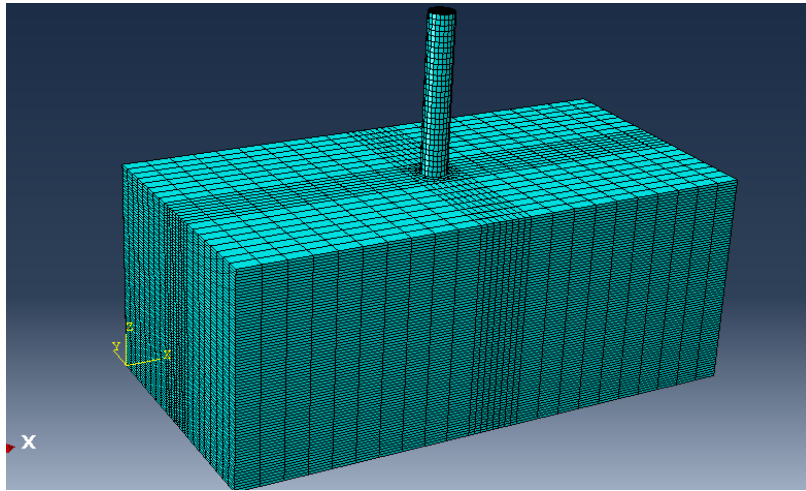


Figure 31: FEM Mesh

The FEM mesh elements used in this study for soil and pile are C3D8R Hexahedral brick elements with reduced integration. The details of the mesh are given in table 8

Table 8: Detail of Mesh

Element	Element Type	Number of elements	Number of nodes
Pile	C3D8R	1920	38715
Soil	C3D8R	34200	2501
Total		36120	41216

4.2.2 Relationship between Depth and Bending Moment

For the FEA performed, the graphs between depth and bending Moment for the angle of internal friction 30° are shown in the subsequent figures.

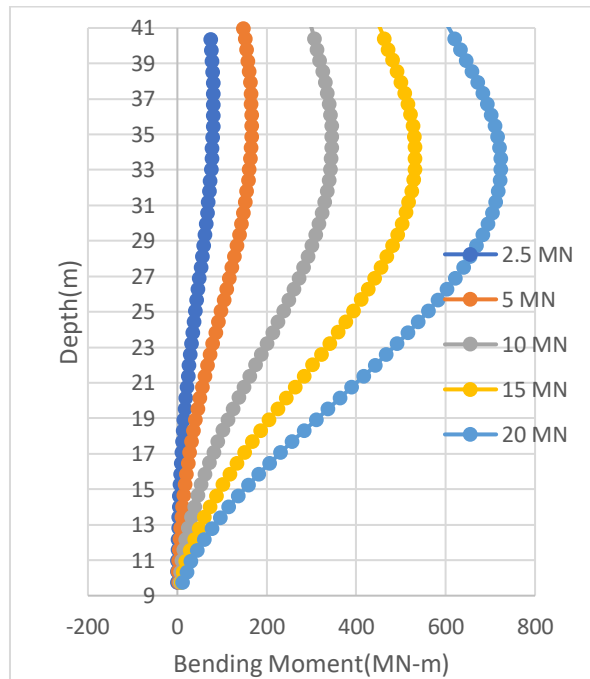


Figure 32: The relationship between depth and bending Moment for the angle of internal friction 30°

For the FEA performed, the graphs between the P-soil reaction and the depth for the angle of internal friction 35° are shown in the subsequent figures.

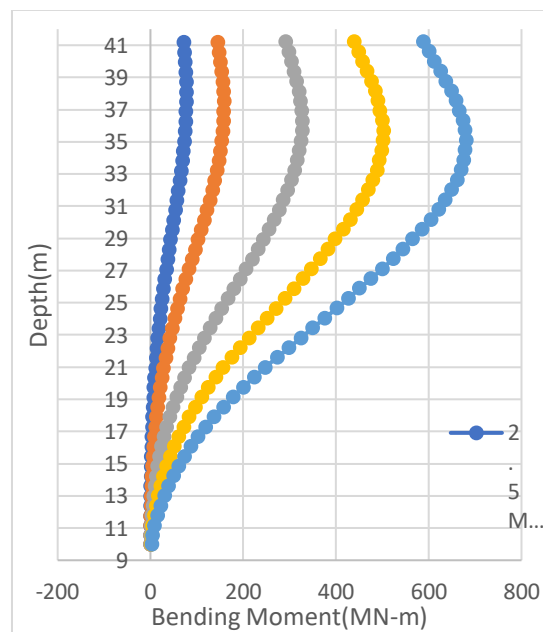


Figure 33: The relationship between depth and bending Moment for the angle of internal friction 35°

For the FEA performed, the graphs between the P-soil reaction and the depth for the angle of internal friction 40° are shown in the subsequent figures.

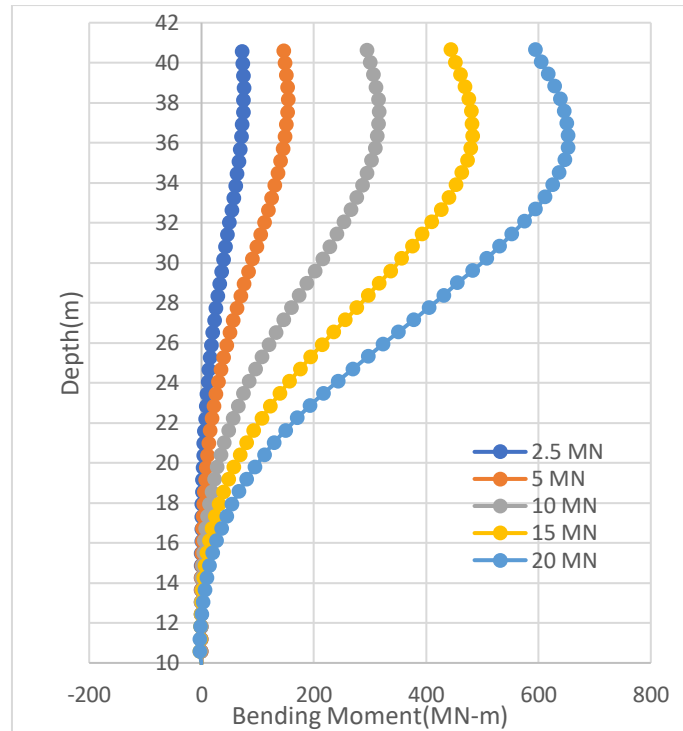


Figure 34: The relationship between depth and bending Moment for the angle of internal friction 40°

4.2.3 Relationship between depth and displacement

As stated earlier for the results of 3m diameter, as the monopile is embedded deeper into the soil, the displacement tends to decrease. This is because the deeper embedment provides a larger soil volume to resist the lateral and vertical loads acting on the monopile. Deeper embedment increases the bearing capacity of the soil, leading to reduced lateral and vertical displacements. Same results are observed in this case of 5m diameter

For the FEA performed, the graphs between the depth and displacement for the angle of internal friction 30° are shown in the subsequent figures.

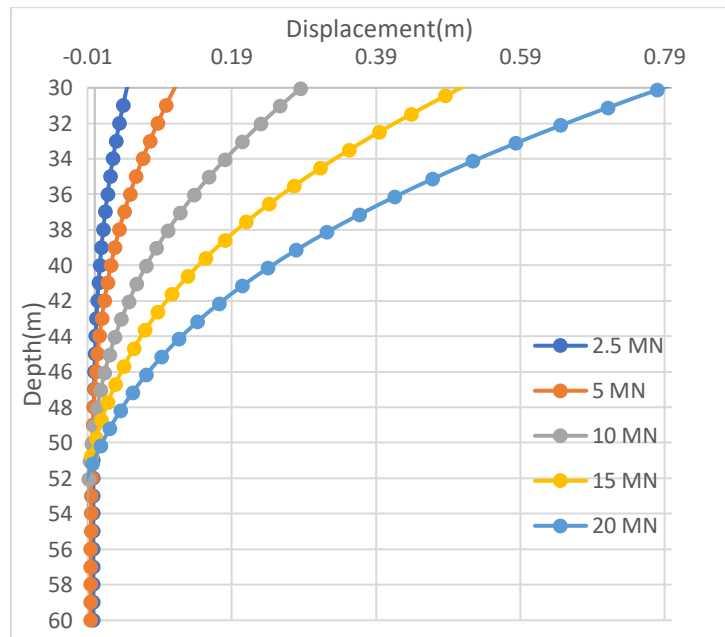


Figure 35: The relationship between depth and displacement at for the angle of internal friction 30°

For the FEA performed, the graphs between the depth and displacement for the angle of internal friction 35° are shown in the subsequent figures.

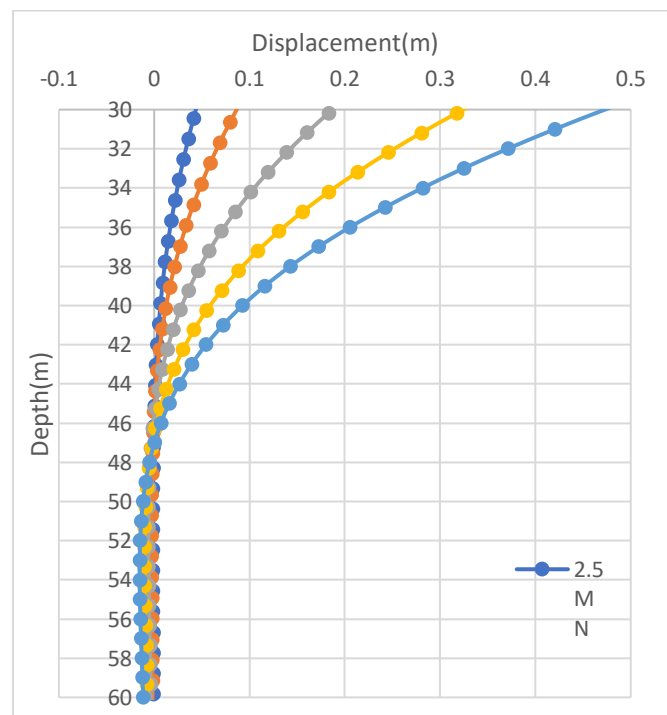


Figure 36: The relationship between depth and displacement at for the angle of internal friction 35°

For the FEA performed, the graphs between the depth and displacement for the angle of internal friction 40° are shown in the subsequent figures.

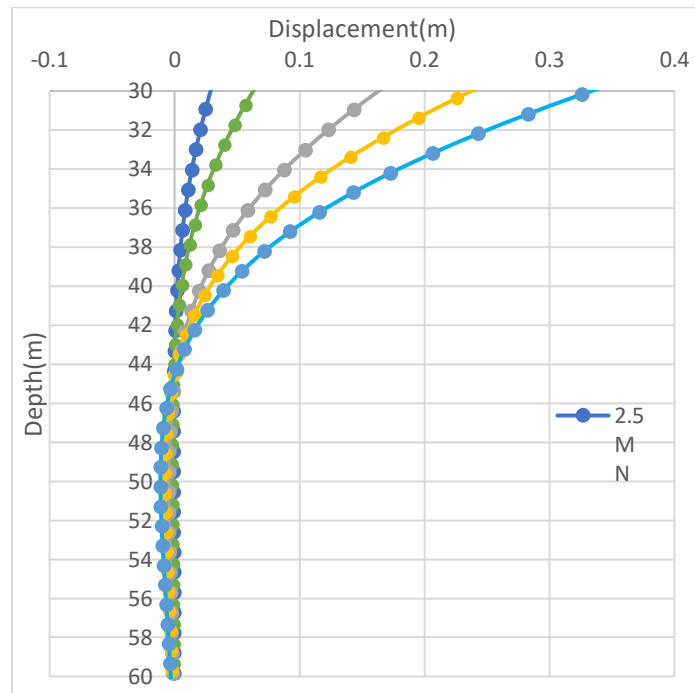


Figure 37: The relationship between depth and displacement at for the angle of internal friction 40°

4.2.4 P-Y Curves

In numerical simulations, *P-Y* curves are derived by modeling the monopile and surrounding soil. The properties of the soil, such as stiffness, strength, and nonlinear behavior, are considered to create an accurate representation of the soil-pile interaction. The numerical model is then subjected to lateral loading, and the resulting pile deflections and soil reactions are used to develop the *P-Y* curves.

For the FEA performed, the P - Y curves for the angle of internal friction 30° are shown in the subsequent figures.

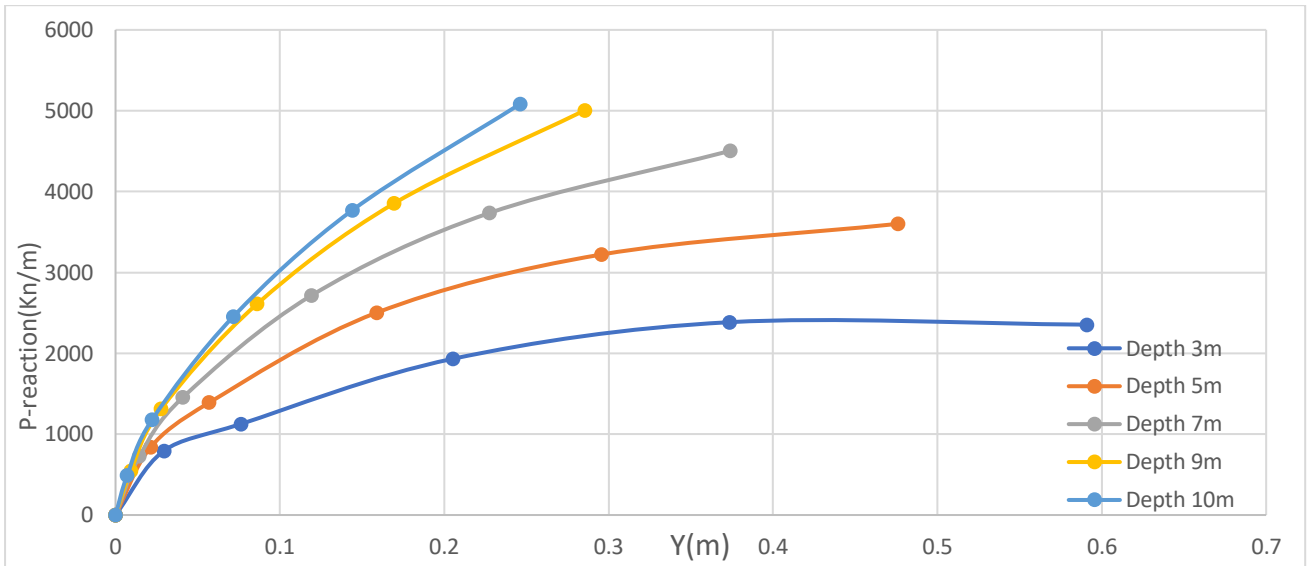


Figure 38: The P - Y Curves for the angle of internal friction 30°

For the FEA performed, the P - Y curve for the angle of internal friction 35° are shown in the subsequent figures.

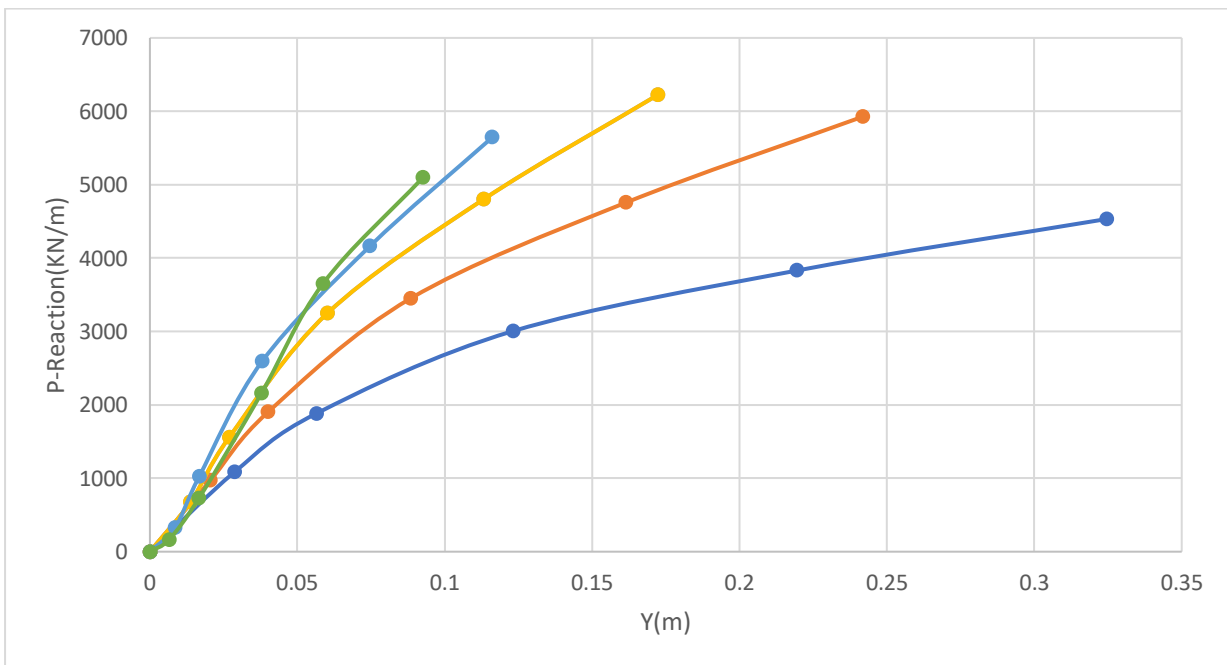


Figure 39: The P - Y Curves for the angle of internal friction 35°

For the FEA performed, the P - Y curves for the angle of internal friction 40° are shown in the subsequent figures.

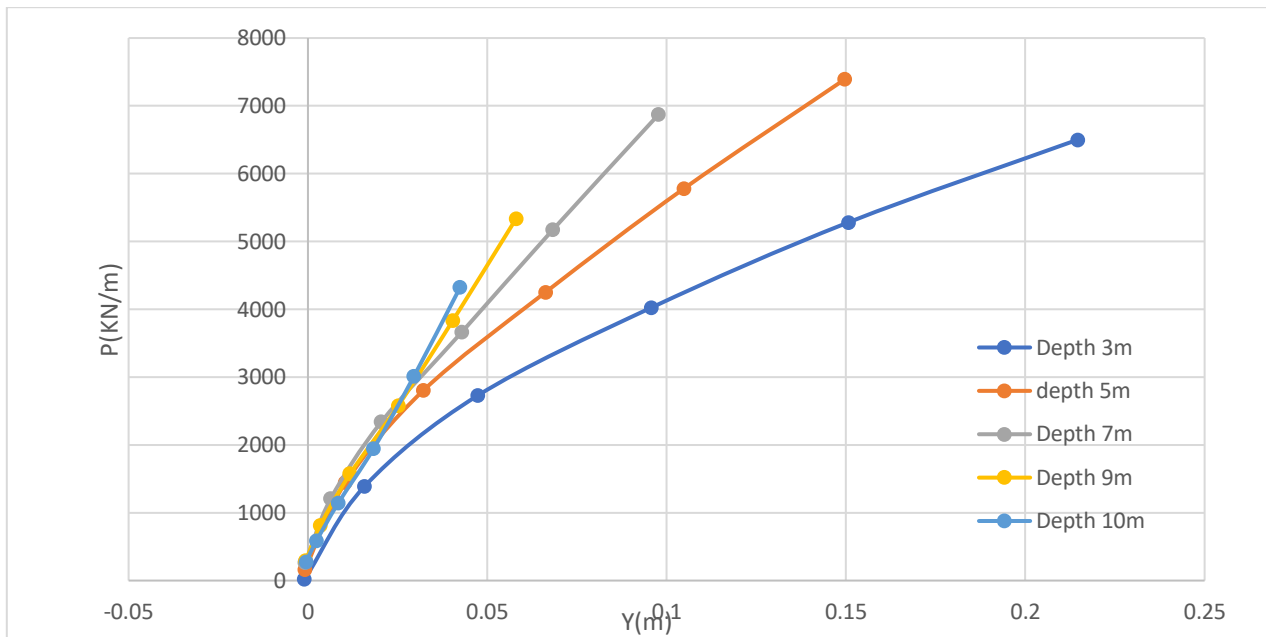


Figure 40: The P - Y for the angle of internal friction 40°

As the depth increases, the P - Y curves are becoming more linear, indicating that lateral loads have much less impact at greater depths than the near-ground surface. Therefore P - y curves for depths of 3, 5 and 7 meters where P -reaction is maximum for the lateral load of 2.5, 10 and 15 MN are more critical for the design consideration of monopile with a diameter of 7 meters in given soil and loading conditions.

4.3 FEM Analysis of 7m diameter:

4.3.1 General Properties

The soil profile considered for this parametric study was sand consisting of 40 layers each layer with a thickness of 1 meter. The sand was modeled as an elastic perfectly plastic material with Mohr-Coulomb failure criterion.

The coefficient of friction for the pile-soil interface (μ) was set to 0.4. The elastic modulus of soil varied from 9.064 MPa for the first layer to 80.56 MPa for the last layer because of the effect of overburden pressure.

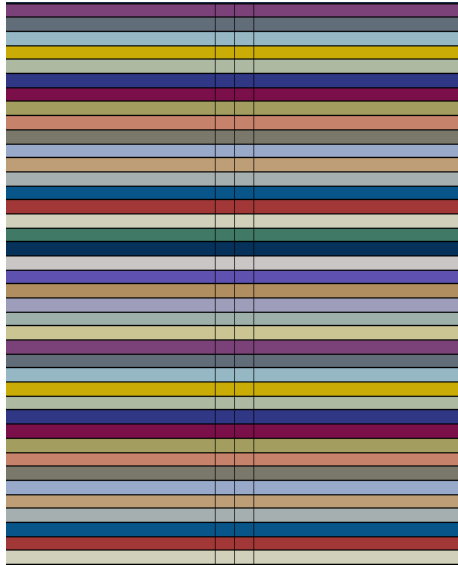


Figure 41: The 40 layers of the soil from top to bottom with increasing elastic modulus

The structural properties of the pile are given in the table 9

Table 9: Properties of piles

Pile Structural Element	Values
Diameter	7 meters
Total length	60 meters
Embedded length	30 meters
L/D ratio	8.57
Elastic Modulus	13 GPa

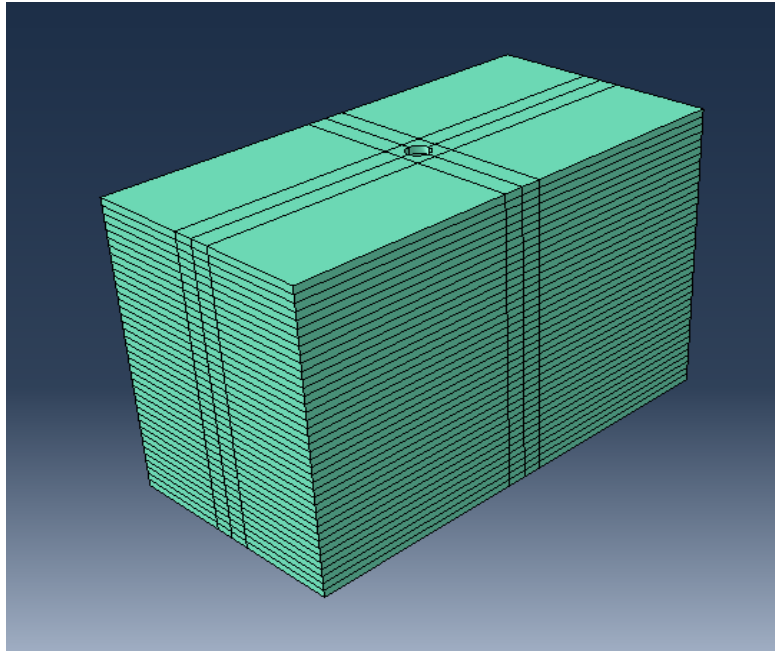


Figure 42: FEM Mesh

The FEM mesh elements used in this study for soil and pile are C3D8R Hexahedral brick elements with reduced integration. The details of the mesh are given in table 10

Table 10: Detail of Mesh

Element	Element Type	Number of elements	Number of nodes
Pile	C3D8R	1920	38715
Soil	C3D8R	34200	2501
Total		36120	41216

4.3.2 Relationship between depth and bending moment

For the FEA performed, the graphs between the bending moment and the depth for the angle of internal friction 30° are shown in the subsequent figures.

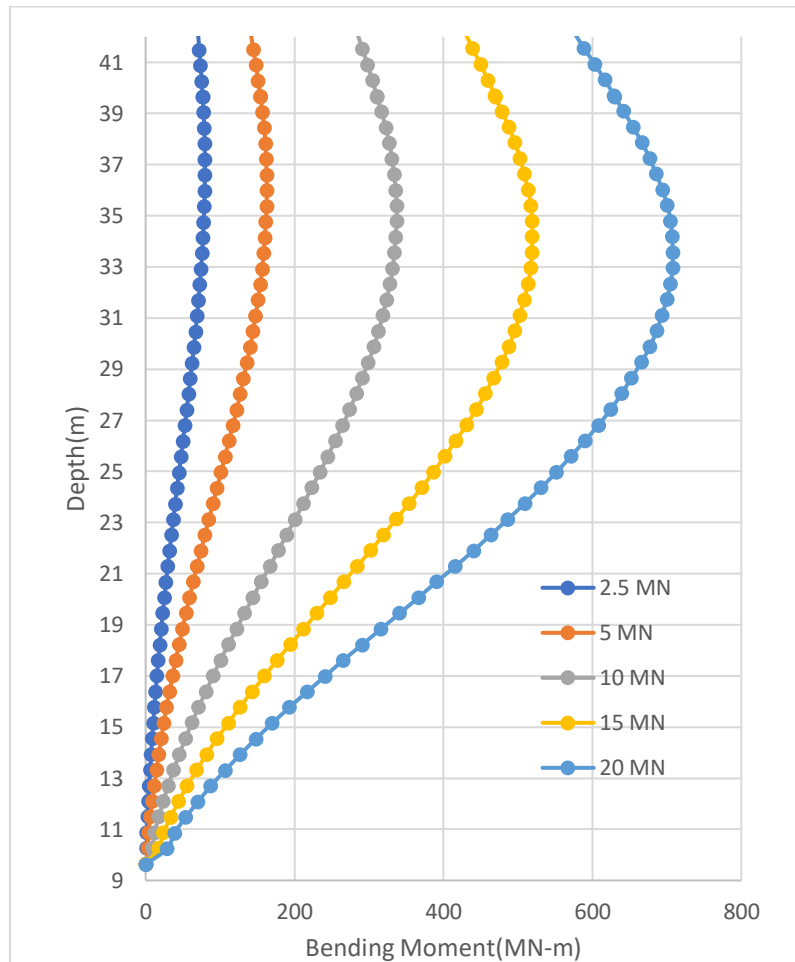


Figure 43: The relationship between the bending moment and the depth for the angle of internal friction 30°

For the FEA performed, the graphs between the bending moment and the depth for the angle of internal friction 35° are shown in the subsequent figures.

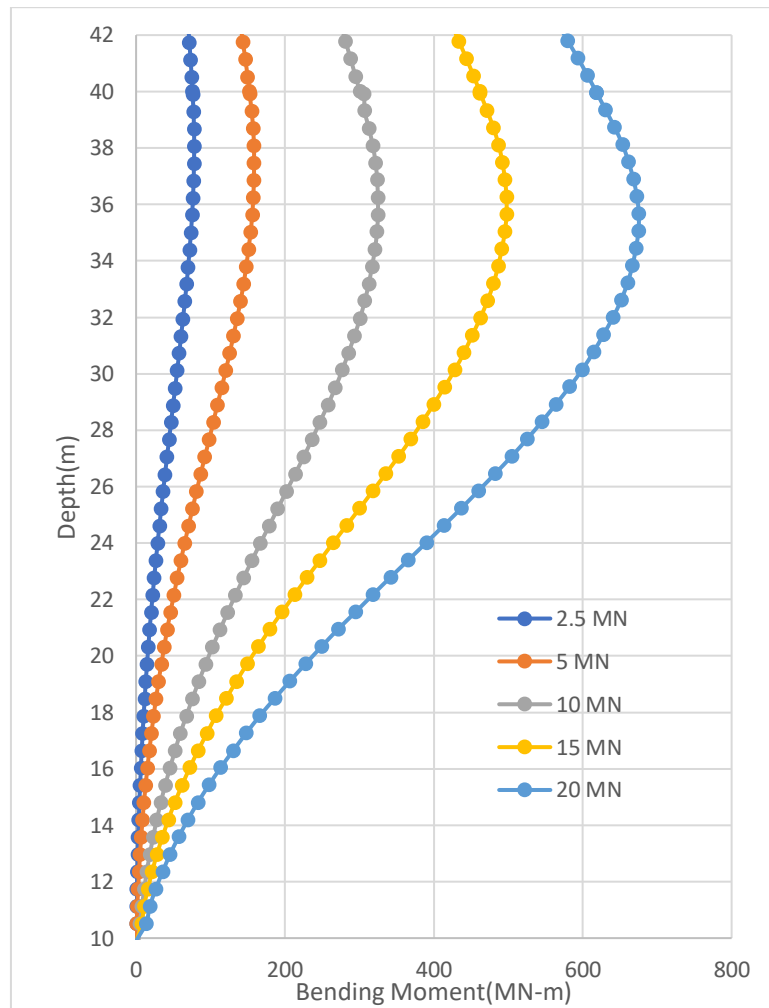


Figure 44: The relationship between the bending moment and the depth for angle of internal friction 35°

For the FEA performed, the graphs between the depth and the bending moment for the angle of internal friction 40° are shown in the subsequent figures.

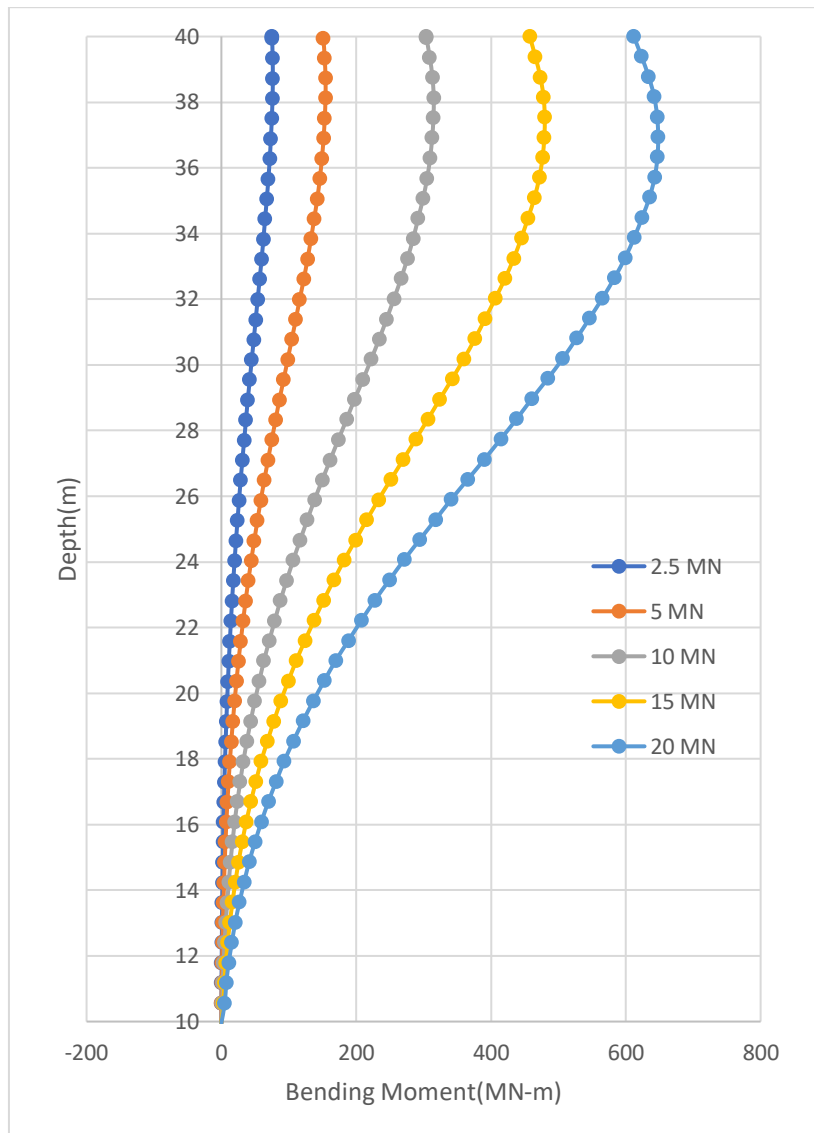


Figure 45: The relationship between the bending moment and the depth for the angle of internal friction 40°

4.3.3 Relationship between depth and displacement

For the FEA performed, the graphs between the depth and displacement for the angle of internal friction 30° are shown in the subsequent figures.

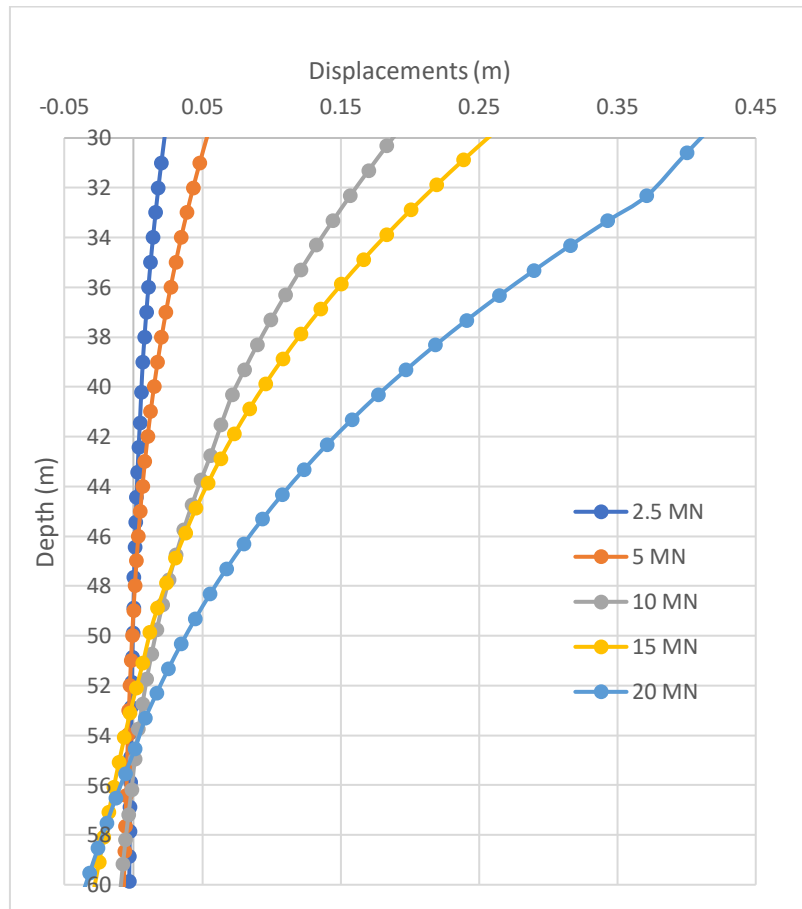


Figure 46: The relationship between depth and displacement at for the angle of internal friction 30°

For the FEA performed, the graphs between the depth and displacement for the angle of internal friction 35° are shown in the subsequent figures.

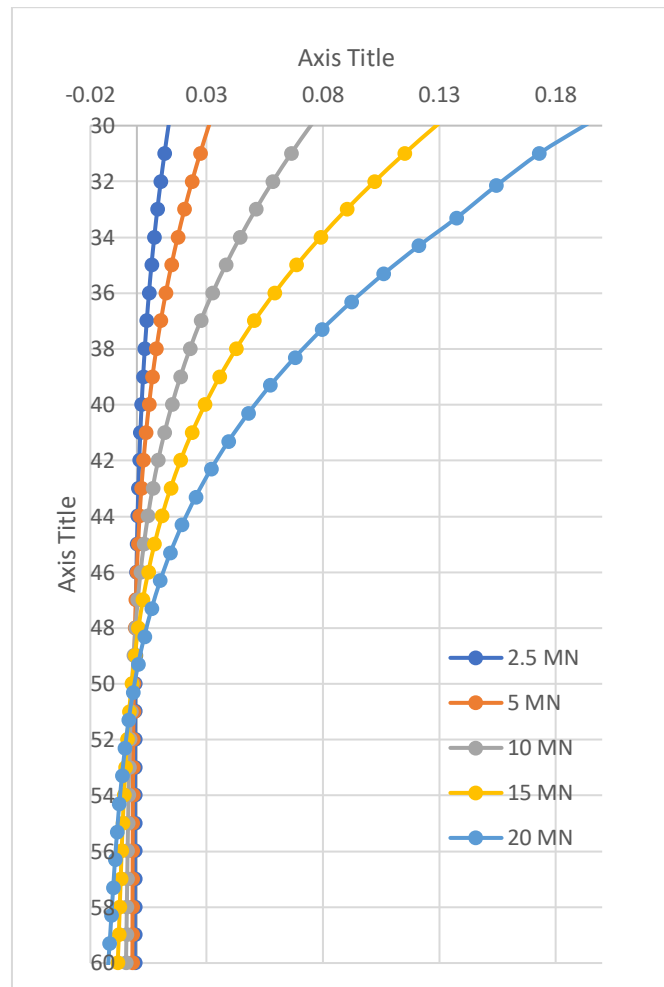


Figure 47: The relationship between depth and displacement at for the angle of internal friction 35°

For the FEA performed, the graphs between the depth and displacement for the angle of internal friction 40° are shown in the subsequent figures.

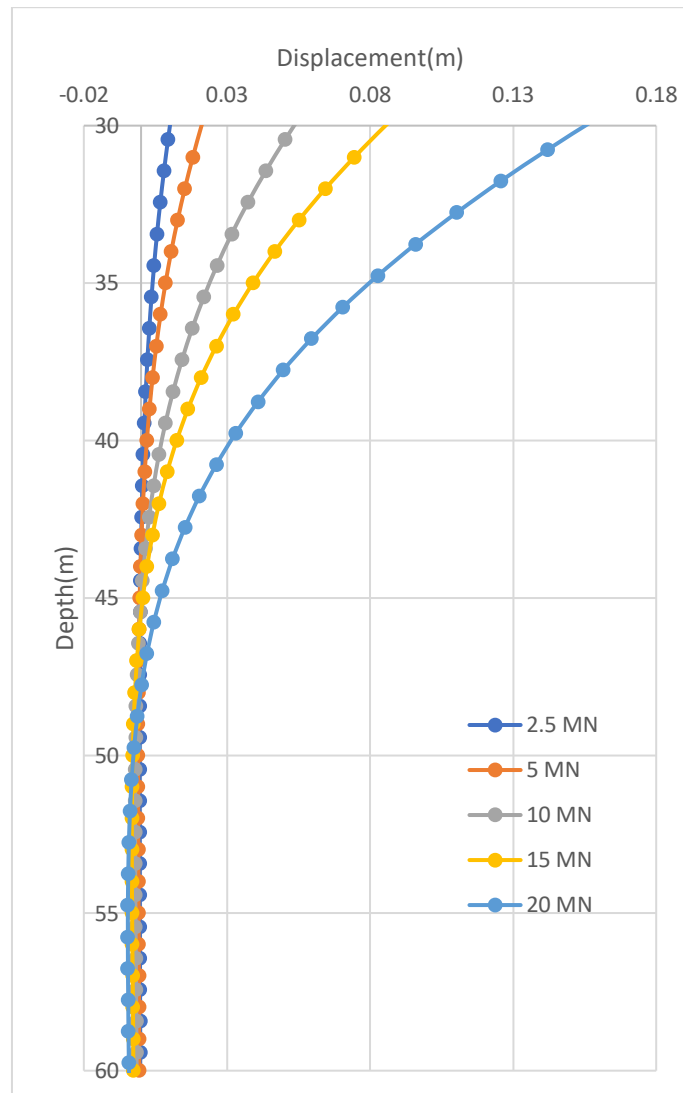


Figure 48: The relationship between depth and displacement at for the angle of internal friction 40°

4.1.4 P-Y Curves.

For the FEA performed, the P-Y curves for the angle of internal friction 30° are shown in the subsequent figures.

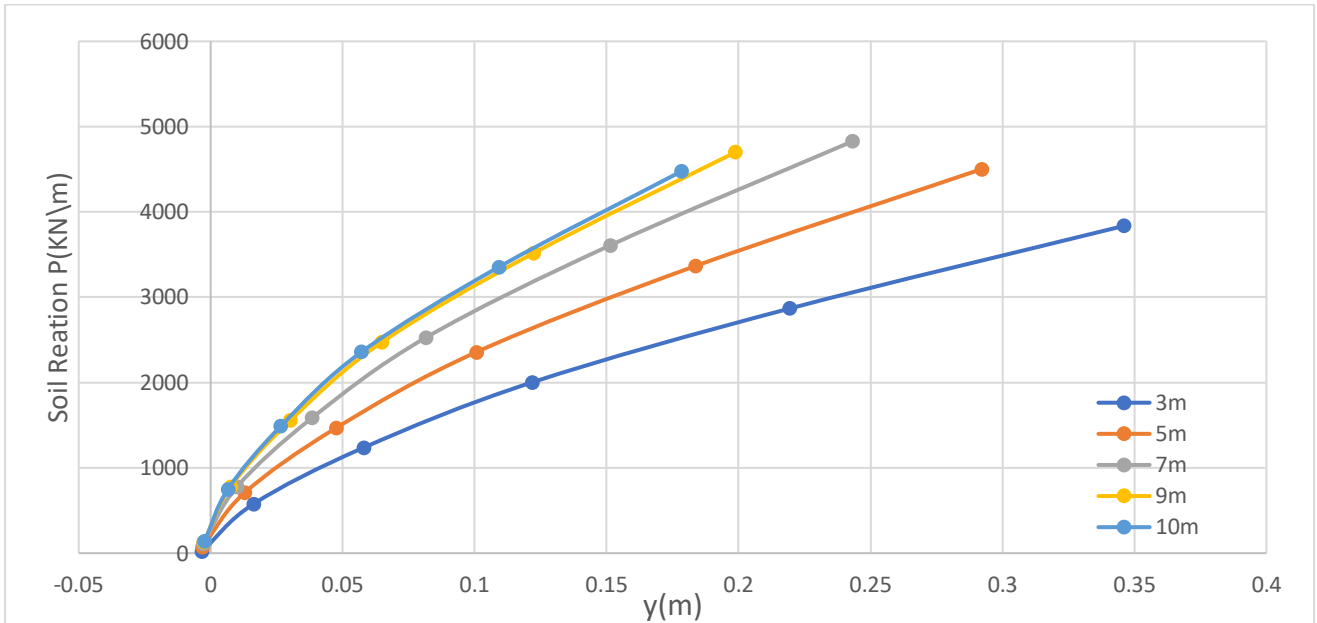


Figure 49: The P-Y Curves for the angle of internal friction 30°

For the FEA performed, the P-Y curves for the angle of internal friction 35° are shown in the subsequent figures.

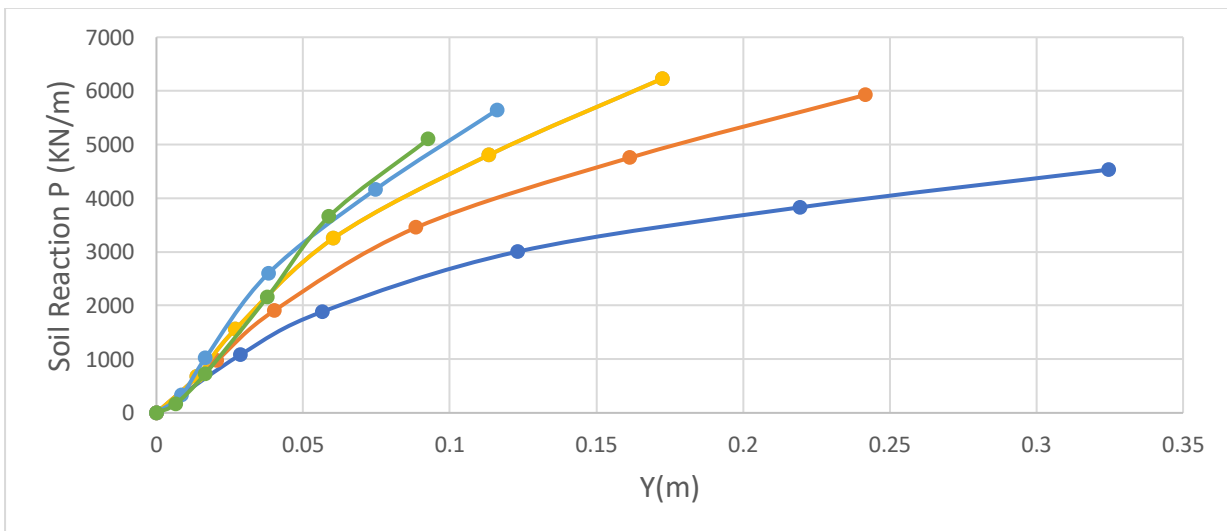


Figure 50: The P-Y Curves for the angle of internal friction 35°

For the FEA performed, the P - Y curves for the angle of internal friction 40° are shown in the subsequent figures.

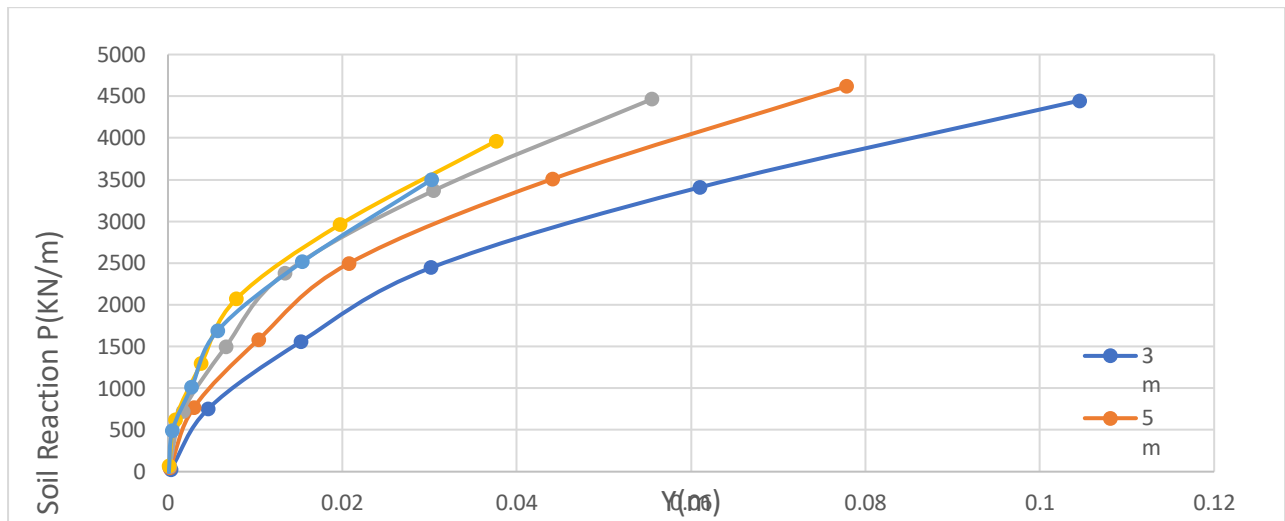


Figure 51: The P - Y at for the angle of internal friction 40°

As the depth increases, the P - Y curves are becoming more linear, indicating that lateral loads have much less effect at greater depths than the near-ground surface. Therefore P - y curves for depths of 3, 5 and 7 meters where P -reaction is maximum for the lateral load of 2.5, 10 and 15 MN are more critical for the design consideration of monopile with a diameter of 7 meters in given soil and loading conditions.

Recommended Equation:

The curve of best fit is used to mathematically describe and summarize the relationship between variables in your data. While the original P-Y curves may provide valuable information, fitting a curve to the data allows you to derive a concise mathematical equation that represents the general trend and behavior of the data points.

The curve of best fit serves several purposes:

- a) **Concise Representation:** It provides a mathematical equation that summarizes the relationship between the variables of interest, such as deflection and soil resistance. This equation can be used to make predictions or estimate values beyond the range of the original data.
- b) **Visualization:** Overlaying the curve of best fit on the P-Y curves plot allows for a visual comparison between the fitted curve and the original data points. This helps to assess how well the fitted curve captures the overall trend and variability in the data.
- c) **Interpolation and Extrapolation:** The curve of best fit allows you to estimate values between the data points (interpolation) and beyond the range of the original data (extrapolation). This can be useful when you need to estimate the behavior of the system at unmeasured deflection values or predict the soil resistance at larger deflections.
- d) **Parameter Interpretation:** The fitted parameters in the equation of the curve of best fit, such as the scaling factor and the rate of change, provide insights into the underlying processes or physical mechanisms driving the relationship between the variables. These parameters can be analyzed to gain a deeper understanding of the system.

In summary, while the original P-Y curves provide the raw data, fitting a curve of best fit allows for a compact representation, improved visualization, and enhanced interpretability of the relationship between variables. It enables extrapolation, interpolation, and the extraction of key parameters for further analysis and decision-making

5.1 Parameters for 3 m

By finite element analysis of 3m diameter of a monopile, the p-y curves were generated for 30°,35°,40° for five different loading conditions. The plot was imported in originpro and further analysis for the curve of best fit was found,

The most suitable function, which best fitted the curve, was:

$$y = a \times x^b$$

Where, the parameters for various points are shown in the table below

Depth (m)	EQUATION		$y = a \times x^b$			
	30°		35°		40°	
	A	b	A	b	a	b
3	3844.3241	0.3558	5316.56452	0.4099	9129.00978	0.5591
5	5533.7512	0.4498	7429.85616	0.4928	16499.4238	0.6707
7	6928.4337	0.4995	9440.86924	0.5696	21929.3368	0.6549
9	9196.6208	0.66	11927.6984	0.6945	32428.6412	0.7469
10	8866.9687	0.6384	13670.8714	0.7784	37417.2436	0.7595

Table 11: The permissible values of constants a and b in the general form of equation of best fit

Depth (m)	EQUATION			$y = a \times x^b$					
	30°			35°			40°		
	Reduced Chi-Sqr	R-Square (COD)	Adj. R-Square	Reduced Chi-Sqr	R-Square (COD)	Adj. R-Square	Reduced Chi-Sqr	R-Square (COD)	Adj. R Square
3	136792.704	0.918	0.890	46273.825	0.987	0.983	59690.380	0.992	0.990
5	38809.697	0.991	0.989	15946.573	0.998	0.997	102546.844	0.994	0.992
7	15853.664	0.998	0.997	27389.395	0.997	0.996	43109.354	0.997	0.996
9	68811.860	0.991	0.988	101467.569	0.988	0.984	22984.487	0.998	0.997
10	4494.800	0.999	0.999	170360.479	0.977	0.970	6090.625	0.999	0.999

Table 12: The values of statistical parameters to justify the correctness of the results 5.2 Parameters for 5m

After detailed analysis on Originpro and by performing number of iterations it was shown that the same equation best fits the p - y curve, the following tables provide a detailed description of various statistical parameters to be used as the proof for correctness of the basic equation, The most suitable function, which best fitted the curve, was:

$$y = a \times x^b$$

Where, the parameters for various points are shown in the table below

Depth (m)	EQUATION		$y = a \times x^b$			
	30°		35°		40°	
	A	b	A	b	a	B
3	3374.699	0.41976	8980.089	0.56587	16172.1	0.59081
5	5582.812	0.48503	16352.52	0.68599	25431.58	0.65238
7	8097.125	0.54541	26001.94	0.79048	36880.14	0.72609
9	11025.03	0.60628	40830.76	0.90327	55711.44	0.83027
10	12487.34	0.6279	73174.59	1.108	75759.91	0.91515

Table 13: The permissible values of constants a and b in the general form of equation of best fit

Depth (m)	EQUATION			$y = a \times x^b$					
	30°			35°			40°		
	Reduced Chi-Sqr	R-Square (COD)	Adj. R-Square	Reduced Chi-Sqr	R-Square (COD)	Adj. R-Square	Reduced Chi-Sqr	R-Square (COD)	Adj. R-Square
3	45489.8	0.93496	0.91329	35573.32	0.98643	0.9819	1079.536	0.9998	0.99974
5	36889.35	0.98008	0.97344	57350.43	0.98948	0.98597	10442.58	0.99858	0.99811
7	26724.51	0.99177	0.98903	78699.28	0.98861	0.98482	28322.2	0.99579	0.99438
9	14621.35	0.99668	0.99557	87960.8	0.98628	0.98171	34509.38	0.99206	0.98941
10	6092.927	0.9987	0.99826	72097.47	0.98705	0.98274	29397.61	0.99017	0.98689

Table 14: The values of statistical parameters to justify the correctness of the results

5.3 Parameters for 7m

After detailed analysis on Originpro and by performing number of iterations it was shown that the same equation best fits the p-y curve, the following tables provide a detailed description of various statistical parameters to be used as the proof for correctness of the basic equation, The most suitable function, which best fitted the curve, was:

$$y = a \times x^b$$

Where, the parameters for various points are shown in the table below

Depth (m)	EQUATION		$y = a \times x^b$			
	30°		35°		40°	
	A	b	A	b	a	B
3	7505.211	0.63141	9202.913	0.49896	9202.913	0.49896
5	9603.775	0.61505	12901.68	0.52323	12901.68	0.52323
7	11295.59	0.60056	17840.44	0.55598	17840.44	0.55598
9	12056.28	0.58256	22978.06	0.58121	22978.06	0.58121
10	12051.82	0.57379	24852.7	0.58784	24852.7	0.58784

Table 15: The permissible values of constants a and b in the general form of equation of best fit

Depth (m)	EQUATION			$y = a \times x^b$					
	30°			35°			40°		
	Reduced Chi-Sqr	R-Square (COD)	Adj. R-Square	Reduced Chi-Sqr	R-Square (COD)	Adj. R-Square	Reduced Chi-Sqr	R-Square (COD)	Adj. R-Square
3	215.469	0.9999	0.99987	23970.74	0.98714	0.98392	23970.7382	0.98714	0.98392
5	746.4147	0.99975	0.99967	20280.18	0.99229	0.99036	20280.1759	0.99229	0.99036
7	1425.071	0.99959	0.99945	16339.62	0.995	0.99375	16339.6166	0.995	0.99375
9	1887.33	0.99941	0.99922	15639.09	0.99535	0.99418	15639.0909	0.99535	0.99418
10	1876.721	0.99936	0.99914	16432.98	0.9947	0.99337	16432.9772	0.9947	0.99337

Table 16: The values of statistical parameters to justify the correctness of the results

5.4 Equation

After detailed analysis on Originpro and by performing number of iterations it was shown that the same equation best fits the p-y curve The most suitable function, which best fitted the curve, was:

$$y = a \times x^b$$

Where, the parameters for various points are shown in the above table

It is to be noted that the value of coefficient of determination (R-squared) has a value for all the parameters, greater than 0.95 and in most cases, it is so close to 1. It is a statistical fact that the higher the value of R squared the more accurate the result is hence it is evident to claim that the equation proposed is the best fit for 3m, 5m and 7m diameter and for the depths of 3m to 10m which are the most critical depths to design and analyze the structure.

Validation

The process of evaluating the accuracy, reliability, and the effectiveness of a model under study is called validation. It determines whether the obtained results are valid, which means that they precisely and accurately present the intended concept or a phenomenon.

6.1 Aims and Objectives of Validation:

- To ensure the accuracy and soundness of the results obtained from the numerical simulation.
- To enhance the credibility and the solidity of the results.
- To assess the generalizability and the relevance of the research findings.
- Establishing the basis for decision-making based on the evidences.

6.2 Finite Element Analysis:

Finite element analysis is a numerical method that is used for the simulation and the analysis of complex engineering structures. To carry out the finite element analysis field tests were performed in the Pearl River Estuary. The soil consists of two layers the upper layer is soft clay and the other layer is sand. To acquire the undrained shear strength (S_u) for soft clay, unconsolidated, undrained, triaxial compression tests (UU tests), cone penetration tests (CPT) and unconfined compression tests were performed. To calculate the elastic modulus (E) for each layer of soft clay, an empirical relation proposed by the Professional Standards Compilation Group of the People's Republic of China was used:

$$S_u = 0.04q_c + 2 \text{-----} (6.1)$$

The results obtained using the empirical relation for cone resistance (q_c) were then used to calculate the elastic modulus. The relation used to calculate the elastic modulus for soft clay is:

$$E = (4 \times q_c) + 5000 \text{-----} (6.2)$$

The test pile was open ended and was composed of Q345 steel that has elastic modulus of 213GPa. Since the pile is hollow in its nature, to model the pile, the elastic modulus was adjusted using the relationship:

$$ES_{solid}I_{solid} = ES_{hollow}I_{hollow} \text{-----} (6.3)$$

The pile had density of 7850 kg/m³ and a Poisson's ratio of 0.3. The pile was discretized by C3D8R Hexahedral brick elements.

6.3 Soil Modelling

The soil profile considered for this experimental study was clay consisting of 24 layers each layer with a thickness of 1 meter and last layer with thickness of 1.5m and sand consisting of 45 layers each layer with a thickness of 1 meter and last layer with thickness of 1.5m. The clay and sand were modeled as an elastic perfectly plastic material with Mohr-Coulomb failure criterion. The details are shown in table 17

Table 17: Properties of sand and clay

	Clay	Sand
Properties	value	value
Mass density (ρ)	6.7 (KN/m ³)	9.36 (KN/m ³)
Poisson Ratio (ν)	0.42	0.30
Angle of internal friction (θ)	12.5 °	35 °
Angle of dilation (Ψ)	0 °	5°
Cohesion yield stress	14	100

The coefficient of friction for the pile-soil interface (μ) was set to 0.4. The elastic modulus of clay varied from 5.5 MPa for the first layer to 6.6 MPa for the last layer and for sand it was 87.7 MPa for first layer and 182.9 MPa for last layer because of the effect of overburden pressure

The figure 53 shows the 69 layers the soil from top to bottom with increasing elastic modulus.

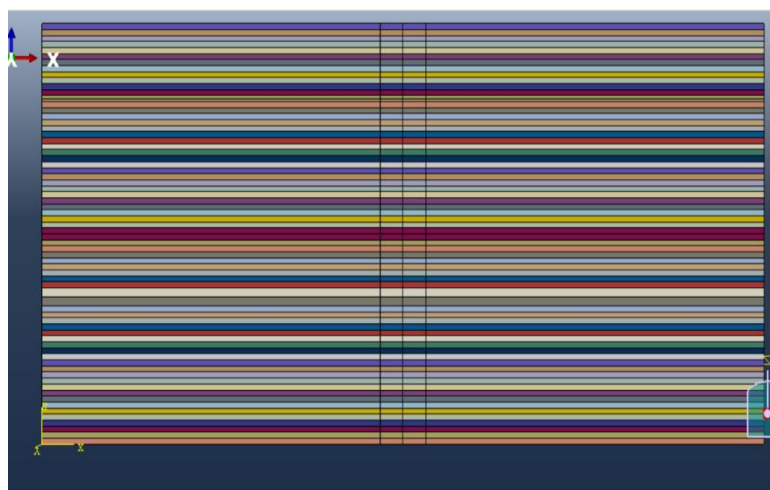


Figure 52: Layers of soil

6.4 Pile Modelling

The steel pile of 2.2-meter diameter used by zhu et al for his experimental study had following properties. The pile model was made considering these properties of the pile shown in table 18

Table 18: Properties of pile

Pile structural elements	Value
Diameter (D)	2.2 meters
Thickness	0.03 meters
Total Length	70 meters
Total Embedded length (L)	57.4 Meters
Embedded Clay length (L ₁)	24.5m
Embedded Sand length (L ₂)	32.9m
Elastic modulus	202 Gpa
Poisson ratio (ν)	0.3

6.5 FE Mesh

The FEM mesh elements as shown in figure 54 used in this study for soil and pile are **C3D8R** Hexahedral brick elements with reduced integration.

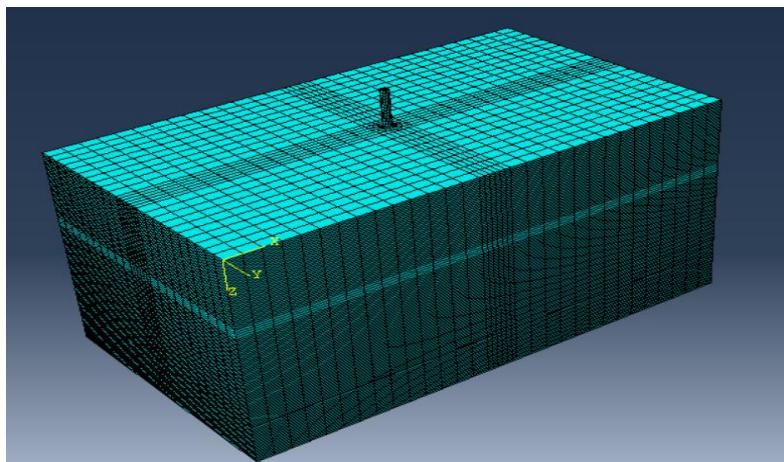


Figure 53: Finite element mesh

The details of the mesh are given in table 19

Table 19: Mesh Details

	Element type	No. of elements	No. of Nodes
Pile	C3D8R	2272	2808
Soil	C3D8R	125,900	136,170
Total		128,172	138,978

6.6 Loading:

The analysis was done on a pile with a diameter of **2.2m** under different lateral loads which as given below

Table 20: Loadings

Sr.no	Load (MN)
1	0.3
2	0.6
3	1.0
4	1.3
5	1.7
6	2.0

6.7 Boundary Conditions:

The x- and y-directional movement of the nodes on the soil perimeter was restricted. The whole soil's base was exposed restrained in all three directions by using the Pin-connection, while the on the faces in the x and y direction were restrained using roller support condition. To prevent the pile from moving downwards during the application of gravity loads, the roller support condition was established the x and y direction around pile, they were deactivated while the lateral load was applied.

6.8 Comparison of Experimental and FEA results:

In this section, the results obtained from the numerical analysis are compared with experimental results under subject of different loads. Moment versus depth, displacement versus depth and the P-Y curves are compared below:

6.8.1 Relationship between depth and bending moment

The graph attached below shows the comparison of displacement against depth under action of different loads, between the numerically and experimentally obtained results:

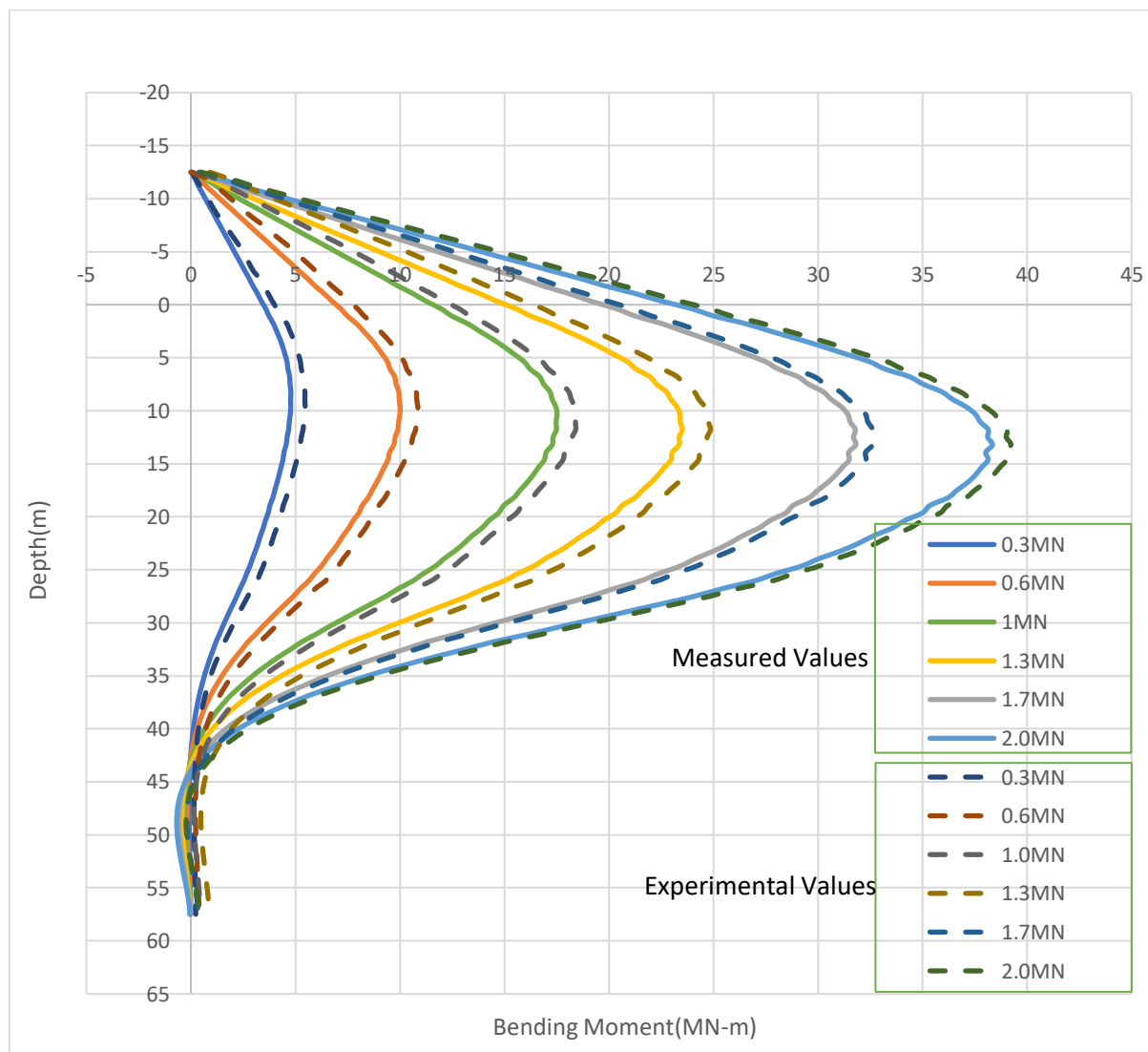


Figure 54: Comparison of bending moment and depth curve between the experimental study results and Finite element analysis results

6.8.2 Relationship between depth and displacement:

The graph attached below shows the comparison of displacement against depth under action of different loads, between the numerically and experimentally obtained results:

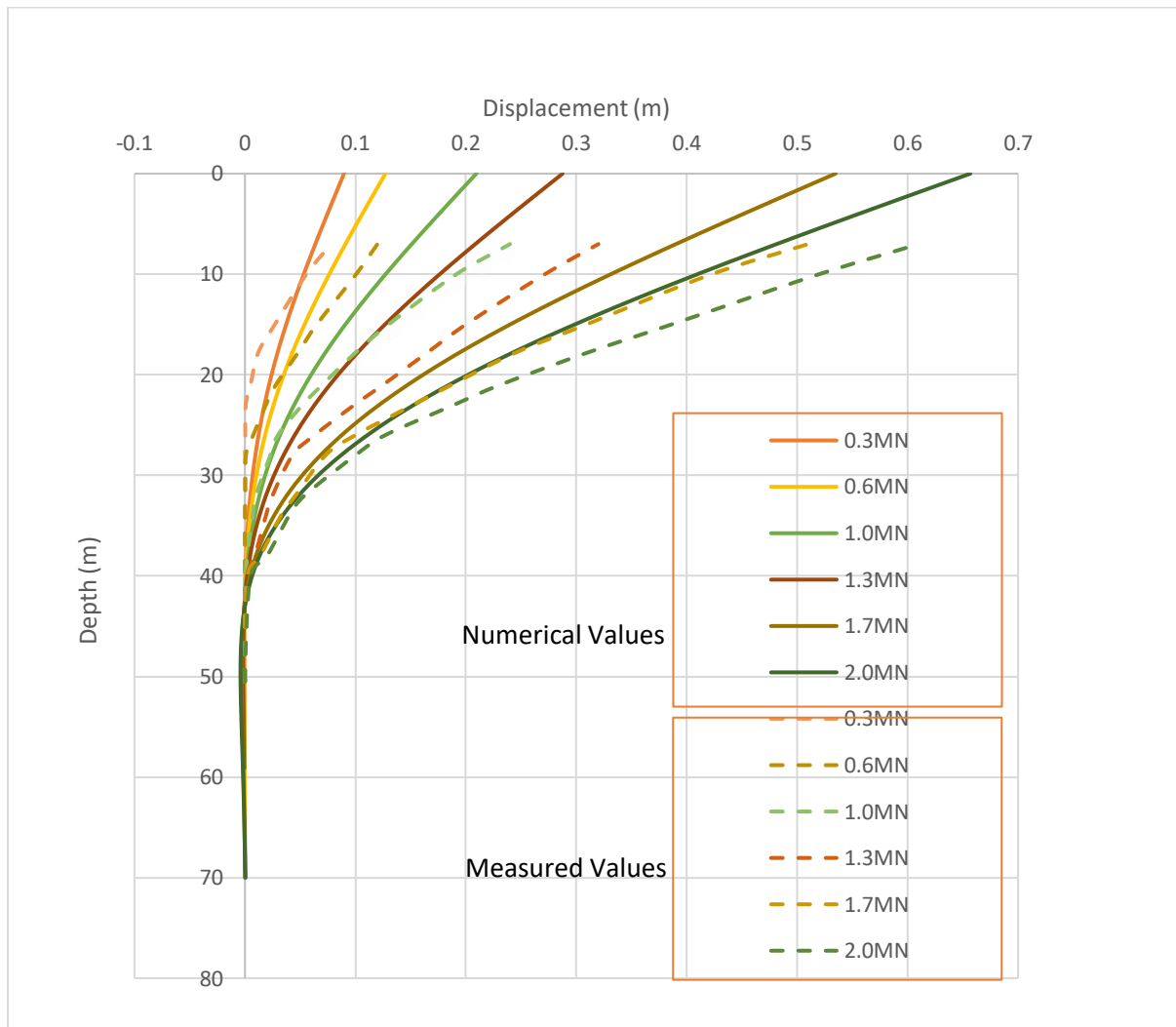


Figure 55: Comparison of depth and displacement curve between the experimental study results and Finite element analysis results

6.8.3 P-Y Curves

The graph attached below shows the comparison of P-Y curve, between the numerically and experimentally obtained results:

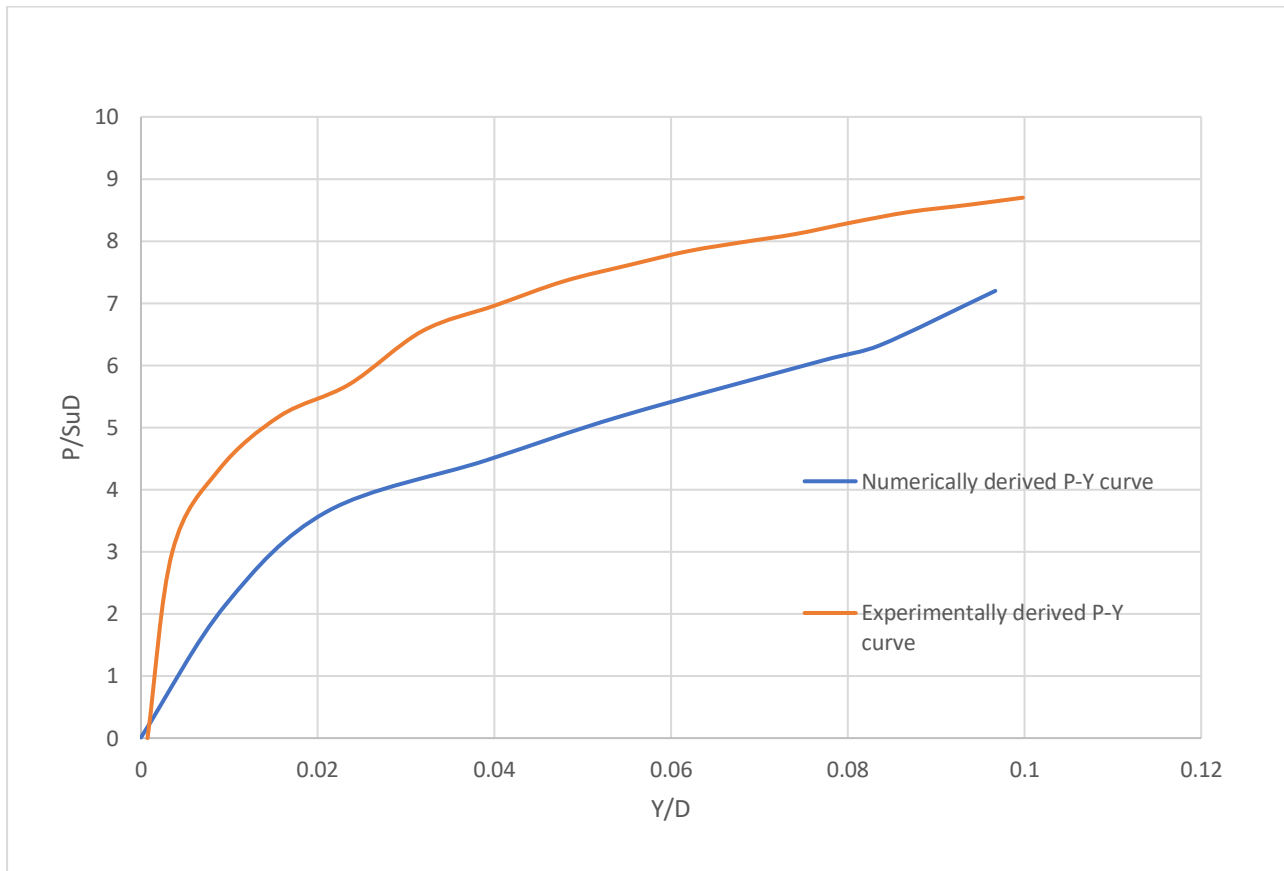


Figure 56: Comparison of p-y curves of experimental study and Finite element analysis

6.9 Results and analysis:

It can be seen from the compared graphs that the experimentally derived values for moment and displacement are equal to the graphs obtained from the numerical analysis. The moment graphs dictate that the difference between the experimentally derived values and the numerically derived values ranges from 3-7% that is acceptable. From displacement versus depth graphs, it could be noticed that the difference between the experimentally derived values and the numerically derived values, is very less ranging from 2-5%. Similarly, P-Y curve at depth of $Z=1D$ below ground surface, is plotted and compared with the experimentally obtained P-Y curve. The results show that the difference is much less.

Since the results are obtained using the Mohr Coulomb criteria and the comparison manifest that the results are much closer to the experimental results. Thus, it could be said that the obtained results are valid, which means that they precisely and accurately present the intended concept or a phenomenon.

Conclusion

7.1 Relationship between depth and bending Moment:

It is observed in all the bending moment and depth (embedded length) curves, after the application of lateral loads, and with the increase in pile diameter, the position of bending moment of the pile is shifted from 3-6 times of the diameter to the pile top and then it tends to decrease and the bending moment at the top of the pile is zero. The pile top function as a free end and the pile end is embedded in the stiff soil so the bending moment tends to move from the pile body to pile top.

7.2 Relationship between depth and displacement:

After a detailed FEA analysis of 3m, 5m and 7m diameter of a monopile, it is observed that in all cases, the greater application of load has given a greater value of deflection, but there is a certain trend followed by the shape of the graph, It is to be noticed that the at the point where the first interaction of soil and pile take place the value of deflection is very large and it tends to decrease as the depth increases, the main reason behind this is the gradual increase in the young modulus of the soil with an increase of 1 meter in depth as the soil became stiffer the holding power starts to increase which lead to this trend.

7.3 Relationship between soil resistance and displacement:

P-y curves were the final result of all FEA's, the graph plotted for soil resistance and lateral displacement show a greater agreement with the general trend of p-y curves. The soil reaction rapidly increased until the displacement of 7-11 mm was reached. A non-linear behavior is observed. The main reason for this impact is that the initial soil resistance has a significant impact on the shape of p-y curves. Initially for small deflections, the lateral soil resistance increased linearly with deflection . As the deflection increases further, the resistance starts to reach the peak. This peak point is the ultimate resistance. The shape of the p-y curves reflects the nonlinear behavior of the soil-pile system. Initially, for small deflections, the lateral soil resistance increases linearly with deflection. As the deflection increases further, the resistance starts to reach a peak and then gradually decreases. The point at which the resistance peaks is often referred to as the ultimate resistance.

7.4 Potential Contributions:

This research provides a very efficient solution for the energy crisis of Pakistan. The world has acknowledged the use the renewable energy resources. Pakistan should consider the use of such a never-ending resource. This parametric study will surely leave an impact for the future researchers and foundation designers to consider the valuable output. In regard to this, there are some notable

observations which this project and study will bring to social, political, and economic culture of Pakistan

- a) With the development of p-y curves for the larger diameter monopiles, the offshore wind energy sector will witness the significant growth which will contribute to the substantial increase in the renewable energy adoption
- b) The mass deployment of the OWTs has potential to give an economic boost to the waving economy of Pakistan. It will result in huge employment growth at the marine site, the virgin coastline will start to contribute to the energy sector and help the economy to stabilize
- c) The installation of OWTs in the coastal areas will enhance the dependence over renewable energy resources and, the impact of global warming will reduce to a greater level. This research is linked to one the weapon of fight against climate change
- d) More research in this domain will yield more cost-effective and efficient designs.
- e) Global collaboration with the greater economies will improve the status to Pakistan considering the impact of global warming and grooming economy

7.5 Future Outlook

This parametric study will surely pave the way for the future researchers to add a greater value to this innovative idea. The potential research gaps and future endeavors for the upcoming researchers, the subsequent sections provide a brief introduction and input to this idea which can make this idea more practical, and more shortcomings could be overcome.

Following are the potential research gaps:

- a) The optimization of structural parameters such as pile diameter, thickness and length this will reduce cost saving and will improve the performance of offshore wind turbines.
- b) On going research in the field of material invention can be used to design a monopile foundation with more durable materials, which can reduce the maintenance requirement and improve the overall cost effectiveness.
- c) Considering site specific inputs will increase the practicality of the idea. The original wind speed and wave speed can be used to calculate the real loads and the geotechnical reports of the seabed soil can help to give me idealistic results.
- d) Incorporation of dead load on the wind turbine to check the punching of the foundation effect
- e) Cost analysis of the wind turbine farms and feasibility studies for the construction of the farms in coastal areas of Pakistan

- f) The design of the transition piece that holds the turbine and the pile together,
- g) The life-span analysis and environmental impacts of decommissioning of the system.

References

- Electricity shortfall in Pakistan: <https://tribune.com.pk/story/2370175/electricity-shortfall>.
- Pakistan Coastal Development through Integrated coastal zone management (ICZM), [https://www.pc.gov.pk/uploads/pub/Pakistan Coastal Development ICZM.pdf](https://www.pc.gov.pk/uploads/pub/Pakistan%20Coastal%20Development%20ICZM.pdf)
- Pakistan Meteorological Department (PMD) report: [https://www.pc.gov.pk/uploads/pub/Pakistan Coastal Development ICZM.pdf](https://www.pc.gov.pk/uploads/pub/Pakistan%20Coastal%20Development%20ICZM.pdf)
- US Department of Energy Report, All About Offshore Wind Turbine Foundations
- <https://blog.virtuosity.com/all-about-offshore-wind-turbine-foundations>
- Broms, B. B. (1964). Lateral Resistance of Piles in Cohesionless Soils. *Journal of the Soil Mechanics and Foundations Division*, 90(3), 123–156.
- DNV-GL-AS. (2016). *DNVGL-ST-0126: Support structures for wind turbines*. Det Norske Veritas group.
- Murchison, J., & O'neill, W. (1984). valuation of p-y Relationships in Cohesionless Soils: Analysis and design of pile foundations. *Proceedings of Symposium in Conjunction with the ASCE National Convention, San Francisco, CA. ASCE*, 174–191.
- Murphy, G., Igoe, D., Doherty, P., & Gavin, K. (2018). 3D FEM approach for laterally loaded monopile design. *Computers and Geotechnics*, 100, 76–83. <https://doi.org/10.1016/j.compgeo.2018.03.013>
- Reese, Lymon C., Cox, W. R., & Koop, F. D. (1974). Analysis of Laterally Loaded Piles in Sand. *OTC-2080-MS*.
- Reese, Lymon C, & Matlock, H. (Eds.). (1956). *Non-dimensional solutions for laterally loaded piles with soil modulus assumed proportional to depth*. Association of Drilled Shaft Contractor
- Y. Zhang, K. H. Andersen, and G. Tedesco, “Ultimate bearing capacity of laterally loaded piles in clay e Some practical considerations,” *Mar. Struct.*, vol. 50, pp. 260–275, 2016.
- B. Byrne *et al.*, “New design methods for large diameter piles under lateral loading for offshore wind applications,” *Front. Offshore Geotech. III*, pp. 705–710, 2015.
- M. W. Murchison, J. M. and O'Neill, “Evaluation of P-y relationships in cohesionless soils,” in *Analysis and design of pile foundations, Proceeding, Geotechnical Engineering Division*, 1984, p. 174–192.

- M. W. O'Neill and J. M. Murchison, "An Evaluation of p-y Relationships in Sands. Research Report No. GT-DF02-83," in *Department of Civil Engineering, University of Houston, Houston, Texas, USA.*, 1983.
- L. Reese and R. Welch, "Lateral loading of deep foundations in stiff clay.," *J. Geotech. Geoenvironmental Eng. 101(ASCE 11456 Proceeding).*, 1975.
- Bukhari, I. A., Abro, S. A., & Ghaffar, S. (2019). Investigation of bearing capacity and settlement of monopile foundations in sandy soils. *Geomechanics and Engineering*, 17(6), 515-528.
- Khan, N. H., & Akram, J. (2019). Finite element analysis of monopile foundation for offshore wind turbines in the coastal areas of Pakistan. *Journal of Engineering and Applied Sciences*, 38(2), 193-199.
- Rehman, S., Hasan, M. A., Ali, S., & Ghaffar, S. (2021). Modified design of monopile foundation for offshore wind turbines in the coastal areas of Pakistan. *Energies*, 14(7), 2009.
- BNWF Approach <https://www.researchgate.net/figure/General-view-of-a-beam-on-nonlinear-Winkler-foundation-model-for-nonlinear-dynamic>.
- Gil Rueda, M. (2021). An alternative p-y model for the simulation of large diameter offshore monopiles for wind turbines founded on granular soils under monotonic and cyclic loading
- Naggar, M. H. E., Shayanfar, M. A., Kimiaei, M., & Aghakouchak, A. A. (2005). Simplified BNWF model for nonlinear seismic response analysis of offshore piles with nonlinear input ground motion analysis. *Canadian Geotechnical Journal*, 42(2), 365-380.
- Heidari, Mehdi & El Naggar, Mohamed & El-sawy, Moustafa. (2017). Nonlinear seismic response analysis of single pile in sand
- Elliott, D. South Asia Regional Initiative for Energy Cooperation, and development (SARI-Energy): Wind Resource Assessment and Mapping for Afghanistan and Pakistan; National Renewable Energy Laboratory: Golden, CO, USA. Available online: https://nawabi.de/power/wind/afgpak_wind_nrel.pdf (accessed on 21 May 2007).
- Sheikh Sharif Ahmed, Bipul Hawaladar and Kshama. Roy Finite element modelling of large diameter monopile in dense sand for offshore wind turbine foundation (May 2015)
- Reese, Lymon C, & Matlock, H. (Eds.). (1956). *Non-dimensional solutions for laterally loaded piles with soil modulus assumed proportional to depth*. Association of Drilled Shaft Contractors.
- McClelland, B., & Focht, J. (1956). Soil Modulus for Laterally Loaded Piles. *Journal of the Soil Mechanics and Foundations Division*, 82(4), 1–22.

- Cox, W. R., Reese, L. C., & Grubbs, B. R. (1974, January 1). *Field Testing of Laterally Loaded Piles in Sand*. Offshore Technology Conference. <https://doi.org/10.4043/2079-MS>
- Reese, Lymon C., Cox, W. R., & Koop, F. D. (1974). Analysis of Laterally Loaded Piles in Sand. *OTC-2080-MS*.
- Murchison, J., & O' eill, W. (1984). valuation of p - y Relationships in Cohesionless Soils: Analysis and design of pile foundations. *Proceedings of Symposium in Conjunction with the ASCE National Convention, San Francisco, CA. ASCE*, 174–191.
- B. Krishnaveni, Satya Kiran Raju Alluri and M.V. Ramana Murthy Generation of P - Y curve for large diameter monopiles through numerical modelling. (July 2016)
- Tushar Raktate and Rohan Choudhary Design of Monopile Foundation for Offshore Wind Turbine. (June 2021)
- API. (2014a). *API RP 2A-WSD: Planning, Designing and Constructing Fixed Offshore Platforms—Working Stress Design* (22nd ed.). American Petroleum Institute.





Digital Receipt

This receipt acknowledges that Turnitin received your paper. Below you will find the receipt information regarding your submission.

The first page of your submissions is displayed below.

Submission author: RTP .
Assignment title: RTP
Submission title: FYP SYN#11
File name: Final_thesis_Monopiles.pdf
File size: 3.68M
Page count: 89
Word count: 17,265
Character count: 99,560
Submission date: 01-Jun-2023 08:43AM (UTC-0700)
Submission ID: 2106778397



**BE CIVIL ENGINEERING
PROJECT REPORT**

Modified Design of Monopiles for the offshore wind turbines (OWT) in the coastal areas of Pakistan

Project submitted in partial fulfillment of the requirements for the degree
of
BE Civil Engineering

PROJECT ADVISOR
Lt. Col. Dr. Naveed Meta
PROJECT CO-ADVISOR
AP Dr. Muhammad Bilal Adeel

SYNDICATE MEMBERS

Muhammad Usama khan (Syndicate Leader)	293927
Muhammad Sayyam Asif	290289
Muhammad Abdullah	298126
Abdul Muhaimin Jamil	287028
Zia Ur Rehman	297400
Ali Hassan	309533

i

ORIGINALITY REPORT

15%

SIMILARITY INDEX

10%

INTERNET SOURCES

12%

PUBLICATIONS

4%

STUDENT PAPERS

PRIMARY SOURCES

1	manglar.uninorte.edu.co Internet Source	2%
2	Yun Wook Choo, Dongwook Kim. "Experimental Development of the p-y Relationship for Large-Diameter Offshore Monopiles in Sands: Centrifuge Tests", Journal of Geotechnical and Geoenvironmental Engineering, 2016 Publication	1%
3	Nassr N. Salman, Mohsen A. Issa. "Displacement Capacities of H-Piles in Integral Abutment Bridges", Journal of Bridge Engineering, 2019 Publication	1%
4	research.library.mun.ca Internet Source	<1%
5	hdl.handle.net Internet Source	<1%
6	acikerisim.deu.edu.tr Internet Source	<1%

7	indico.cern.ch Internet Source	<1 %
8	www.yumpu.com Internet Source	<1 %
9	pdfcoffee.com Internet Source	<1 %
10	www.mdpi.com Internet Source	<1 %
11	Ke Wu. "Finite Element Modeling of Horizontally Loaded Monopile Foundation of Large Scale Offshore Wind Turbine in Non-homogeneity Clay", 2009 WRI World Congress on Software Engineering, 05/2009 Publication	<1 %
12	H. Wang, L.Z. Wang, Yi. Hong, B. He, R.H. Zhu. "Quantifying the influence of pile diameter on the load transfer curves of laterally loaded monopile in sand", Applied Ocean Research, 2020 Publication	<1 %
13	members.cgs.ca Internet Source	<1 %
14	vbn.aau.dk Internet Source	<1 %
15	Cheng Lin, Caroline Bennett, Jie Han, Robert Parsons. "Effect of Soil Stress History on	<1 %

Scour Evaluation of Pile-Supported Bridges",
Journal of Performance of Constructed
Facilities, 2015

Publication

16

Hongwang Ma, Jun Yang, Longzhu Chen.
"Numerical analysis of the long-term
performance of offshore wind turbines
supported by monopiles", Ocean Engineering,
2017

Publication

17

ir.lib.uwo.ca

Internet Source

18

Muniram Budhu. "Nonlinear analysis of
laterality loaded piles in cohesionless soils",
Canadian Geotechnical Journal, 05/1987

Publication

19

projekter.aau.dk

Internet Source

20

www.theses.fr

Internet Source

21

flex.flinders.edu.au

Internet Source

22

Sayed, M.. "A numerical model of iceberg
scour", Cold Regions Science and Technology,
200901

Publication

<1 %

<1 %

<1 %

<1 %

<1 %

<1 %

<1 %

- | | | |
|----|--|------|
| 23 | jddtonline.info
Internet Source | <1 % |
| 24 | link.springer.com
Internet Source | <1 % |
| 25 | www.cee.hawaii.edu
Internet Source | <1 % |
| 26 | www.researchgate.net
Internet Source | <1 % |
| 27 | Bin Zhu, Zhou-jie Zhu, Tao Li, Jin-chao Liu, Yan-feng Liu. "Field Tests of Offshore Driven Piles Subjected to Lateral Monotonic and Cyclic Loads in Soft Clay", Journal of Waterway, Port, Coastal, and Ocean Engineering, 2017
Publication | <1 % |
| 28 | Haoran OuYang, Guoliang Dai, Luchao Gao, Anhui Wang, Weiming Gong. "Lateral response of monopile reinforced by cement-improved soil in clay to monotonic and cyclic loadings: Laboratory model test and theoretical investigation", Marine Structures, 2023
Publication | <1 % |
| 29 | Yun Wook Choo, Dongwook Kim, Jae-Hyun Park, Kiseok Kwak, Jae-Hyun Kim, Dong-Soo Kim. "Lateral Response of Large-Diameter Monopiles for Offshore Wind Turbines from | <1 % |

Centrifuge Model Tests", Geotechnical Testing Journal, 2014

Publication

30

fr.scribd.com

Internet Source

<1 %

31

idoc.pub

Internet Source

<1 %

32

www.tdx.cat

Internet Source

<1 %

33

Submitted to University of Bristol

Student Paper

<1 %

34

collections.mun.ca

Internet Source

<1 %

35

Gi-Chun Kang, Jiseong Kim. "Behavioral Characteristics of Group Batter Piles According to Pile Inclination and Action Direction under Statically Lateral Loads", Journal of Testing and Evaluation, 2018

Publication

<1 %

36

Submitted to University of South Florida

Student Paper

<1 %

37

Youhu Zhang, Knut H. Andersen. "Soil reaction curves for monopiles in clay", Marine Structures, 2019

Publication

<1 %

38 Yueguan Yan, Yanjun Zhang, Yuanhao Zhu, Jinchi Cai, Junyao Wang. "Quantitative Study on the Law of Surface Subsidence Zoning in Steeply Inclined Extra-Thick Coal Seam Mining", Sustainability, 2022
Publication

39 oaktrust.library.tamu.edu
Internet Source

40 "Geohazards", Springer Science and Business Media LLC, 2021
Publication

41 core.ac.uk
Internet Source

42 es.scribd.com
Internet Source

43 seaoi.org
Internet Source

44 Ahmed, Sheikh Sharif, Bipul Hawlader, and Kshama Roy. "Finite Element Modeling of Large Diameter Monopiles in Dense Sand for Offshore Wind Turbine Foundations", Volume 1 Offshore Technology Offshore Geotechnics, 2015.
Publication

45 Philip Alkhoury, Abdul-Hamid Soubra, Valentine Rey, Mourad Ait-Ahmed. "Dynamic

analysis of a monopile-supported offshore wind turbine considering the soil-foundation-structure interaction", Soil Dynamics and Earthquake Engineering, 2022

Publication

46

library.ctr.utexas.edu

Internet Source

<1 %

47

Submitted to Universiti Teknologi Malaysia

Student Paper

<1 %

48

www.ic2e.org

Internet Source

<1 %

49

Hao Wang, Dewei Fu, Tiantian Yan, Deng Pan, Weiwei Liu, Liqun Ma. "Bearing Characteristics of Multi-Wing Pile Foundations under Lateral Loads in Dapeng Bay Silty Clay", Journal of Marine Science and Engineering, 2022

Publication

<1 %

50

Sheikh Sharif Ahmed, Bipul Hawlader, Kshama Roy. "Finite Element Modeling of Large Diameter Monopiles in Dense Sand for Offshore Wind Turbine Foundations", Volume 1: Offshore Technology; Offshore Geotechnics, 2015

Publication

<1 %

51

Submitted to The Hong Kong Polytechnic University

Student Paper

<1 %

52	ijmt.ir Internet Source	<1 %
53	ngi.brage.unit.no Internet Source	<1 %
54	repository.up.ac.za Internet Source	<1 %
55	www.fhwa.dot.gov Internet Source	<1 %
56	"Advances in Construction Materials and Sustainable Environment", Springer Science and Business Media LLC, 2022 Publication	<1 %
57	Submitted to University of Leeds Student Paper	<1 %
58	"Proceedings of China-Europe Conference on Geotechnical Engineering", Springer Science and Business Media LLC, 2018 Publication	<1 %
59	G Wu, WDL Finn. "Dynamic nonlinear analysis of pile foundations using finite element method in the time domain", Canadian Geotechnical Journal, 1997 Publication	<1 %
60	Submitted to Swinburne University of Technology Student Paper	<1 %

61	av333.info Internet Source	<1 %
62	Submitted to Danford College Student Paper	<1 %
63	Submitted to Indian Institute of Technology, Bombay Student Paper	<1 %
64	Shou, K.J.. "Analysis of the Chiufengershan landslide triggered by the 1999 Chi-Chi earthquake in Taiwan", Engineering Geology, 200303 Publication	<1 %
65	Submitted to University of Oklahoma Student Paper	<1 %
66	dspace.nwu.ac.za Internet Source	<1 %
67	www.iitk.ac.in Internet Source	<1 %
68	K.L. Wu. "Optimal all-to-all broadcasting schemes in distributed systems", [1991] Proceedings of the First International Conference on Parallel and Distributed Information Systems, 1991 Publication	<1 %
69	M Hesham El Naggar. "Simplified BNWF model for nonlinear seismic response analysis	<1 %

of offshore piles with nonlinear input ground motion analysis", Canadian Geotechnical Journal, 04/2005

Publication

70

Mingyuan Wang, Miao Wang, Xinglei Cheng, Qun Lu, Jiaqing Lu. "A New p-y Curve for Laterally Loaded Large-Diameter Monopiles in Soft Clays", Sustainability, 2022

Publication

<1 %

71

New Frontiers in Engineering Geology and the Environment, 2013.

Publication

<1 %

72

Submitted to University of Western Sydney

Student Paper

<1 %

73

backend.orbit.dtu.dk

Internet Source

<1 %

74

onlinepubs.trb.org

Internet Source

<1 %

75

repository.charlotte.edu

Internet Source

<1 %

76

www.icevirtuallibrary.com

Internet Source

<1 %

77

Deepak Badoni, Nicos Makris. "Nonlinear response of single piles under lateral inertial and seismic loads", Soil Dynamics and Earthquake Engineering, 1996

Publication

<1 %

78 G. Chortis, A. Askarinejad, L.J. Prendergast, Q. Li, K. Gavin. "Influence of scour depth and type on p-y curves for monopiles in sand under monotonic lateral loading in a geotechnical centrifuge", Ocean Engineering, 2020
Publication <1 %

79 W. D. Liam Finn. "A Study of Piles during Earthquakes: Issues of Design and Analysis", Bulletin of Earthquake Engineering, 01/2005
Publication <1 %

80 Youhu Zhang, Knut H. Andersen, Philippe Jeanjean. "Verification of a framework for cyclic p-y curves in clay by hindcast of Sabine River, SOLCYP and centrifuge laterally loaded pile tests", Applied Ocean Research, 2020
Publication <1 %

81 edoc.pub
Internet Source <1 %

82 escholarship.org
Internet Source <1 %

83 etheses.dur.ac.uk
Internet Source <1 %

84 hrcak.srce.hr
Internet Source <1 %

85 mafiadoc.com

Internet Source

<1 %

86

priodeep.weebly.com

Internet Source

<1 %

87

repository.tudelft.nl

Internet Source

<1 %

88

www.i-asem.org

Internet Source

<1 %

89

www.pc.gov.pk

Internet Source

<1 %

90

Chia-Cheng Fan, James H. Long. "Assessment of existing methods for predicting soil response of laterally loaded piles in sand", Computers and Geotechnics, 2005

Publication

<1 %

91

Krzysztof Trojnar. "Simplified design of new hybrid monopile foundations for offshore wind turbines", Ocean Engineering, 2020

Publication

<1 %

92

Sungmoon Jung, Sung-Ryul Kim, Atul Patil, Le Chi Hung. "Effect of monopile foundation modeling on the structural response of a 5-MW offshore wind turbine tower", Ocean Engineering, 2015

Publication

<1 %

93

Submitted to University of East London

<1 %

94

V. S. Phanikanth, Deepankar Choudhury, G. R. Reddy. "Behavior of Single Pile in Liquefied Deposits during Earthquakes", International Journal of Geomechanics, 2013

Publication

<1 %

95

Xinjun Zou, Xiong Cao, Changlin Zhou, Mi Zhou, Xihong Zhang. "Experimental study on the bearing capacity of large-diameter monopile in sand under water flow condition", Ocean Engineering, 2021

Publication

<1 %

96

Yoo, Min-Taek, Jung-In Choi, Jin-Tae Han, and Myoung-Mo Kim. "Dynamic P-Y Curves for Dry Sand from Centrifuge Tests", Journal of Earthquake Engineering, 2013.

Publication

<1 %

97

Yunhan Huang, Peipei Wang, Ying Lai, Zhongze Xu. "A small-strain soil constitutive model for initial stiffness evaluation of laterally loaded piles in drained marine sand", Ocean Engineering, 2023

Publication

<1 %

98

downloads.hindawi.com

Internet Source

<1 %

99

etd.auburn.edu

Internet Source

<1 %

100 infomar.ie
Internet Source

<1 %

101 repository.lib.ncsu.edu
Internet Source

<1 %

102 s3.eu-central-1.amazonaws.com
Internet Source

<1 %

103 www.dot.nv.gov
Internet Source

<1 %

104 www.igi-global.com
Internet Source

<1 %

105 www.repo.uni-hannover.de
Internet Source

<1 %

106 Ashour, M, G Norris, and J Singh. "Soil-structure interaction in deep foundations", Soil-Foundation-Structure Interaction, 2010.
Publication

<1 %

107 Praveen M. Huded, Suresh R. Dash, Subhamoy Bhattacharya. "Buckling analysis of pile foundation in liquefiable soil deposit with sandwiched non-liquefiable layer", Soil Dynamics and Earthquake Engineering, 2022
Publication

<1 %

108 Sung-Ha Baek, Joonyoung Kim. "Investigation of p-y Behaviors of a Cyclic Laterally Loaded Pile in Saturated Silty Sand", Advances in Civil Engineering, 2022

Publication

<1 %

109 Thieken, Klaus, Martin Achmus, and Kirill Alexander Schmoor. "On the ultimate limit state design proof for laterally loaded piles", geotechnik, 2014.

Publication

<1 %

110 Versteijlen, W G, K N van Dalen, A V Metrikine, and L Hamre. "Assessing the small-strain soil stiffness for offshore wind turbines based on in situ seismic measurements", Journal of Physics Conference Series, 2014.

Publication

<1 %

111 Yaohua Guo, Haijun Wang, Jijian Lian. "Review of integrated installation technologies for offshore wind turbines: Current progress and future development trends", Energy Conversion and Management, 2022

Publication

<1 %

Exclude quotes Off

Exclude matches Off

Exclude bibliography On